CLASSIFICATION:
PHYSICAL SCIENCES: Earth, Atmospheric, and Planetary Sciences

TITLE:
The origin of methanethiol in mid-ocean ridge hydrothermal fluids

SHORT TITLE:
Methanethiol in hydrothermal fluids

AUTHORS & AFFILIATIONS:

Eoghan P. Reeves[a,b,1,2], Jill M. McDermott[a], Jeffrey S. Seewald[a]

[a]Department of Marine Chemistry and Geochemistry, Woods Hole Oceanographic Institution, Woods Hole, MA 02543, U.S.A.

[b]MARUM Center for Marine Environmental Sciences & Department of Geosciences, University of Bremen, Bremen D-28359, Germany

[1]To whom correspondence should be addressed. Email: ereeves@alum.mit.edu

[2]Present address: Department of Earth, Atmospheric and Planetary Sciences, Massachusetts Institute of Technology, Cambridge, MA 02139, U.S.A.

KEYWORDS:
Methanethiol, hydrothermal systems, biogeochemistry

SIGNIFICANCE STATEMENT

Simple alkyl thiols such as methanethiol are widely speculated to spontaneously form in seafloor hot spring fluids, and are implicated in facilitating the emergence of proto-metabolism and microbial life in early Earth hydrothermal systems, the complexation of hydrothermally-derived metals, and as fuels for microbial ecosystems. Existing models suggest that methanethiol forms by non-biological reduction of hydrothermal inorganic carbon (CO_2 or CO). We demonstrate that methanethiol is actively produced in low-temperature mixing zones of hydrothermal systems, but our data suggest it is the thermal destruction of pre-existing organic matter (likely subsurface microbial biomass) that is responsible. Formation of organosulfur compounds and other degradation products during subseafloor mixing may influence the biogeochemistry of low-temperature hydrothermal fluids inhabited by microbial life.

AUTHOR CONTRIBUTIONS:
(E.P.R., J.S.S. designed research; E.P.R., J.M.M., J.S.S. performed research; E.P.R., J.M.M., J.S.S. analyzed data; E.P.R., J.S.S. wrote the paper)

ABSTRACT

Simple alkyl thiols such as methanethiol (CH_3SH) are widely speculated to form in seafloor hot spring fluids. Putative CH_3SH synthesis by abiotic (non-biological) reduction of inorganic carbon (CO_2 or CO) has been invoked as an initiation reaction for the emergence of proto-metabolism and microbial life in primordial hydrothermal settings. Thiols are also presumptive ligands for hydrothermal trace metals and potential fuels for associated microbial communities. In an effort to constrain sources and sinks of CH_3SH in seafloor hydrothermal systems, we determined for the first time its abundance in diverse hydrothermal fluids emanating from ultramafic, mafic and sediment-covered mid-ocean ridge settings. Our data demonstrate that the distribution of CH_3SH is inconsistent with metastable equilibrium with inorganic carbon, indicating production by abiotic carbon reduction is more limited than previously proposed. CH_3SH concentrations are uniformly low (~10^{-8} M) in high-temperature fluids (>200°C) from all unsedimented systems, and in many cases suggestive of metastable equilibrium with CH_4 instead. Associated low-temperature fluids (<200°C) formed by admixing of seawater, however, are invariably enriched in CH_3SH (up to ~10^{-6} M) along with NH_4^+ and low molecular weight hydrocarbons relative to high-temperature source fluids, resembling our observations from a sedimented system. This strongly implicates thermogenic interactions between upwelling fluids and microbial biomass or associated dissolved organic matter during subsurface mixing in crustal aquifers. Widespread thermal degradation of subsurface organic matter may be an important source of organic production in unsedimented hydrothermal systems, and may influence microbial metabolic strategies in cooler near-seafloor and plume habitats.

\body

INTRODUCTION

Since their discovery in 1977, seafloor hot spring fluids have been widely proposed as a potential source of organic molecules necessary for early life to emerge and thrive on a Hadean-Archaean Earth (1-5), and for metabolic energy and fixed carbon in modern hydrothermal systems (6, 7). Abiotic (non-biological) reduction of inorganic carbon (CO_2 or CO) to methanethiol (methyl mercaptan, CH_3SH) is considered a crucial first step in the putative transition from prebiotic to primitive metabolic chemistry, leading to the emergence of hyperthermophilic microbial life (8-13). Specifically, methanethiol is the presumptive abiotic precursor of acetyl thioester (8, 12, 13) - the functional moiety of the Acetyl-CoA co-enzyme central to many ancient metabolic pathways - and a sustainable abiotic source of acetyl thioesters is a key feature of models proposing the emergence of primordial metabolism in hydrothermal settings (5). Alkyl thiols are additionally implicated in the synthesis of the key metabolite pyruvate (10), which is speculated to have lead to a primordial protometabolic network in a hydrothermal setting (14). In modern hot spring environments, hydrothermally-produced thiols could constitute metabolic energy and carbon sources (15) for mesophilic and thermophilic microorganisms in subseafloor, near-vent and plume settings, given that such compounds are intensively cycled in sedimentary microbial habitats (16). Moreover, due to their strong metal-binding abilities, thiol functional groups are also increasingly implicated in the complexation and delivery of hydrothermally-derived metals such as Fe and Cu to the deep ocean (17-19).

Abiotic reduction of inorganic carbon to CH_3SH has been shown to occur under experimental hydrothermal conditions (8, 20, 21) and thermodynamic considerations indicate the abundance of CH_3SH in metastable equilibrium with inorganic carbon sources should increase strongly with dissolved hydrogen (H_2) abundance (22). This has lead to the assumption that CH_3SH should be enriched in H_2-rich fluids emanating from serpentinite-hosted hydrothermal settings, such as the Lost City Hydrothermal Field (13). Without evidence from analogous

48 modern hydrothermal fluids, however, the assumption of widespread thiol production by
49 inorganic carbon reduction in prebiotic seafloor hot springs lacks support.

50 It is generally assumed that low molecular weight organic compounds in hydrothermal
51 fluids emanating from settings lacking significant sedimentary organic matter (unsedimented
52 systems) are primarily derived from inorganic carbon (e.g. mantle-derived CO_2) via abiotic
53 reduction reactions, either by homogeneous reduction or involving heterogeneous mineral
54 catalysts (23). CH_4, C_{2+} hydrocarbons and formate, for example, are postulated to be the products
55 of abiotic carbon reduction in Lost City vent fluids (24, 25). However, potential contributions of
56 thermogenic (i.e. derived from abiotic thermal decomposition of either pre-existing biomass or
57 biologically derived compounds) or biogenic (i.e. derived from metabolic activities of viable
58 organisms) carbon compounds to hydrothermal fluids are poorly constrained at present (7, 26).
59 The fundamental physicochemical processes governing the formation of hydrothermal fluids and
60 the abundances of presumptive inorganic substrates for abiotic synthesis (CO_2/CO, H_2 and H_2S)
61 have likely persisted through geologic time (3), hence diverse modern analogs present an
62 opportunity to assess the potential for abiotic synthesis of CH_3SH on early Earth. Therefore, in
63 order to clarify its production and origin, we investigated the distribution of CH_3SH in 38 hot
64 spring fluids from diverse geologic environments throughout the global mid-ocean ridge system
65 that span a range of temperatures and redox states. Isobaric gas-tight fluid samplers (27) were
66 used to collect the hydrothermal fluids, and the citations for each system included here provide
67 the most relevant or recent reported fluid compositions. Samples were taken from four
68 unsedimented hydrothermal vent fields hosted in basaltic rock: 'Lucky Strike' (28) and 'TAG'
69 (29) on the Mid-Atlantic Ridge (MAR), '9°50'N' (30) on the East Pacific Rise, and 'Piccard' (31,
70 32) on the Mid-Cayman Rise (MCR). Three diverse unsedimented vent fields where
71 serpentinization of ultramafic rock is postulated to influence fluid compositions were sampled:
72 'Lost City' (24) and 'Rainbow' (33) on the MAR, and 'Von Damm' (34) on the MCR. Fluids
73 were also collected from the sediment-hosted 'Guaymas Basin' vent field in the Gulf of

74 California (35, 36), where extensive hydrothermal alteration of organic-rich sediment overburden
75 is occurring. Our results indicate that production of abiotic CH_3SH from inorganic carbon is not
76 occurring to a significant extent, and that abiotic degradation of pre-existing organic matter may
77 instead be the dominant source. The widespread production we observe during crustal mixing of
78 hydrothermal fluids has numerous implications for the biogeochemistry of seafloor hydrothermal
79 systems, which we discuss here.

RESULTS AND DISCUSSION

Measured CH_3SH concentrations vary from approximately 10^{-9} to 10^{-6} M in unsedimented hydrothermal systems **(Table S1)**. In general, low-temperature (<200°C) fluids formed by subsurface mixing of high-temperature endmember fluids with seawater **(*SI Text, Section 1*)** are most enriched. For example, CH_3SH concentrations in mixed fluids at Piccard are above 10^{-6} M, while associated endmember sources are ~10^{-8} M. Cooler endmember fluids at the sedimented Guaymas Basin system contain over 10^{-5} M CH_3SH – the highest concentrations observed, while nearby hotter endmember fluids have abundances similar to most endmember fluids from unsedimented systems (~10^{-8} M). Concentrations are lowest in endmember fluids (94–96°C) of the Lost City Hydrothermal Field (1.4 to 1.9 x 10^{-9} M).

Thermodynamic evaluation of CH_3SH abundances

The abiotic production of CH_3SH in hydrothermal solutions is typically described (13, 22) by the overall reaction of CO_2, H_2 and H_2S according to the relationship:

$$CO_{2(aq)} + H_2S_{(aq)} + 3H_{2(aq)} = CH_3SH_{(aq)} + 2H_2O_{(l)} \quad \textbf{[1]}$$

While CO is also considered a possible substrate for reduction (12, 13, 22), it does not provide an alternate pathway to CH_3SH that is independent of CO_2 reduction in fluids emanating from unsedimented systems. CO is predicted to be maintained at very low abundances due to rapid equilibrium with CO_2 and H_2 (37). Equilibrium between CO_2 and CO is confirmed by calculated chemical affinities near zero for the high temperature vent fluids from unsedimented systems presented in this study **(*SI Text, Sections 2 and 3, Eq. S1 and S2*)**. The stoichiometry of reaction **[1]** indicates that, for a given temperature and pressure, CH_3SH abundance at metastable equilibrium should be highly sensitive to variations in dissolved H_2 due to the third power H_2 dependence of the associated mass action expression. Using measured concentrations of CO_2, H_2 and H_2S and thermodynamic data (22) for reaction **[1]** at measured vent temperatures and pressures, CH_3SH abundances in unsedimented hydrothermal fluids are predicted to vary by over

ten orders of magnitude for metastable chemical equilibrium **(Fig. 1; *SI Text, section 4*)**. Aqueous H_2 concentrations that vary by almost three orders of magnitude, notwithstanding, observed concentrations of CH_3SH are relatively uniform (~10^{-8} M) in high-temperature endmember fluids regardless of the geologic setting **(Fig. 1; Table S1)**. While CH_3SH concentrations below predicted values might suggest kinetic inhibition of reaction **[1]** in high-H_2 fluids (e.g. at Rainbow, Piccard, Von Damm), this does not explain the strongly enriched nature of very H_2-poor fluids relative to predictions (e.g. TAG, Lucky Strike). It is possible that endmember fluids may cool during ascent from higher temperature and pressure subsurface reaction zones, where equilibrium according to reaction **[1]** might regulate CH_3SH abundances. Such a scenario is unlikely, however, as predicted metastable equilibrium concentrations according to reaction **[1]** decrease strongly with increasing temperature (22), which would result in the apparent enrichments in low-H_2 fluids becoming even more pronounced. Collectively, these observations suggest that CH_3SH, CO_2, H_2S, H_2 and H_2O do not attain a state of metastable equilibrium at the diverse conditions encountered by fluids in modern hydrothermal systems. This implies that abiotic synthesis of CH_3SH from inorganic carbon is unlikely, and incapable of sustaining metastable equilibrium abundances.

The relative uniformity of endmember abundances shown in **Fig. 1**, despite widely differing H_2 abundances, suggests CO_2 reduction is not responsible for the production of CH_3SH in high-temperature endmember fluids. Aside from CO_2, methane (CH_4) is invariably the next largest stable pool of dissolved carbon in hydrothermal solutions, with all other aqueous single carbon species representing metastable states (7, 26). Indeed, models that propose reaction **[1]** as the source of CH_3SH in hydrothermal fluids (5, 13, 22) inherently assume metastable CH_3SH is kinetically inhibited from destruction by further reduction to CH_4. For many high-temperature endmember fluids presented here, however, calculated chemical affinities **(*SI Text, Section 2, Eq. S1*)** show CH_3SH is indeed at or close to metastable equilibrium with CH_4 according to the reaction:

$$CH_3SH_{(aq)} + H_{2(aq)} = CH_{4(aq)} + H_2S_{(aq)} \quad \textbf{[2]}$$

For example, affinities for reaction **[2]** for all Rainbow endmember fluids (-3.8 to +0.5 kJ/mol) are within typical uncertainties of equilibrium at conditions of venting **(*SI Text, Section 2*)**. At Piccard (+6.4 to +14.6 kJ/mol) and Lucky Strike (-4.7 to -12.8 kJ/mol), endmembers are also close to equilibrium in several cases, as are some vents at 9°50'N (e.g. 'Tica', +5.5 kJ/mol). Thus, in contrast to reaction **[1]**, measured CH_3SH concentrations in endmember fluids are more consistent with predicted values according to reaction **[2**]. While we cannot exclude that the reverse of reaction **[2]** is occurring, there is to date no evidence to suggest aqueous CH_4 can react with H_2S under hydrothermal conditions. On the contrary, CH_3SH was observed to react to form small quantities of CH_4 at 100°C in the thioester synthesis experiments of Huber and Wächterhäuser (8). Thermodynamic data (22) indicate that reaction **[2]** would maintain CH_3SH at low levels with respect to CH_4 for most hydrothermal fluid compositions, with an inverse dependence on H_2 abundance. This is incompatible with the notion of greater abiotic CH_3SH production with increasing H_2 abundance, as invoked in scenarios for prebiotic hydrothermal thioester production (8, 12, 13). Regardless of whether or not CH_3SH forms by inorganic carbon reduction (reaction **[1]**), or other biogenic or thermogenic processes during hydrothermal fluid circulation, the data presented here strongly suggest that metastable equilibrium with CH_4 at high-temperatures is sufficiently fast that it regulates CH_3SH abundances in endmember fluids according to reaction **[2]**.

Thermogenic CH_3SH production

The highest CH_3SH concentrations were observed in endmember vent fluids from the sediment-covered Guaymas Basin rift zone, where the influence of hydrothermal alteration of immature organic matter and biomass is readily apparent **(Fig. 2)**. At Guaymas Basin, basaltic dikes and sills intrude into 0.5 km-thick organic-rich diatomaceous ooze overlaying the ridge axis, resulting in rapid and widespread hydrothermal alteration of immature sedimentary organic

158 matter and expulsion of hydrothermal petroleum at the seafloor (36, 38). In addition to abundant
159 NH_4^+ and dissolved CO_2, multiple classes of thermogenic organic compounds are added to
160 circulating fluids during this process (35, 36, 39). Alkyl thiols are considered to form
161 predominantly at low thermal maturities during petroleum generation in slowly subsiding
162 sedimentary basins (40), and their production in this setting is therefore not surprising. Cyclic
163 polysulfide organosulfur compounds (thiolanes, thianes, thiepanes) have previously been reported
164 in fragments of an active smoker chimney from Guaymas Basin, indicating organosulfur
165 production during hydrothermal petroleum generation (38). Production of CH_3SH during
166 hydrothermal alteration of sedimentary organic matter could reflect the removal of organosulfur
167 moieties from macromolecular organic structures, or the secondary reaction of thermogenic
168 products such as CO. Indeed, fluids with abundant CH_3SH at Guaymas also have excess CO
169 relative to equilibrium with CO_2 and H_2 **(Table S1; *SI Text, Section 3*)**.

170 The abundance of CH_3SH in fluids at Guaymas Basin is characterized by a bimodal
171 distribution, with cooler endmember fluids being most enriched, and hotter endmember fluids
172 having similarly low abundances to fluids in unsedimented systems. CH_3SH-depleted Rebecca's
173 Roost and Toadstool fluids (288–299°C, **Fig. 2**) have substantially higher $C_1/(C_2+C_3)$ ratios (124–
174 132 versus 55–60) than the CH_3SH-rich cooler fluids (172–251°C), suggesting higher thermal
175 maturity in the hotter fluids, and the conversion of longer chain alkanes to shorter chains (39).
176 These observations suggest that abundant CH_3SH is produced predominantly during early
177 hydrothermal alteration of immature organic matter, consistent with observations from
178 conventional petroleum-producing systems (40). In a similar manner to C_{2+} hydrocarbons, but
179 unlike NH_4^+, CH_3SH may have decomposed (e.g. by reaction **[2]**) at the higher thermal stress of
180 Rebecca's Roost and Toadstool fluids prior to venting.

181 Although significant sedimentary organic matter is lacking at unsedimented spreading
182 centers, the potential still exists for thermogenic production of thiols due to the presence of a
183 putative subsurface biosphere and vent-associated biomass (26, 41-43). In low-temperature

hydrothermal fluids (<200°C) from numerous unsedimented settings, there is substantial evidence to support CH_3SH production during mixing of endmember fluids with seawater within hydrothermal upflow zones or crustal aquifers. Linear mixing relationships between measured Cl and Mg concentrations for fluids sampled at Rainbow, Von Damm, and Piccard indicate that a common source fluid at each vent field feeds all of the overlying vents **(Fig. 3A)**. That many of the replicate fluid samples collected at the low-temperature vents are characterized by nearly identical Mg concentrations implies that mixing of Mg-depleted endmember hydrothermal fluids with Mg-rich seawater occurred in the subsurface prior to sampling, since stochastic admixing of ambient seawater during fluid collection at vent orifices would likely result in highly variable Mg concentrations **(*SI Text, Section 1*)**. In contrast to the conservative behavior that characterizes Cl abundances during mixing, CH_3SH concentrations in mixed fluids are all substantially greater than expected for conservative dilution of the associated high-temperature endmember **(Fig. 3B and Fig. S1)**. Such enrichments require production of CH_3SH during subsurface mixing and associated cooling. While we cannot completely exclude that some component of the CH_3SH in mixed fluids is derived from CO_2 reduction, or abiotic formation from other metastable intermediates, CH_3SH abundances are far below values predicted for metastable equilibrium with respect to CO_2, H_2S, H_2, and H_2O **(Fig. 1)**. It is difficult to argue that reaction **[1]** should only proceed at the lower temperatures and H_2 abundances of mixed fluids, given the complete lack of evidence that inorganic carbon reduction is responsible for CH_3SH production in endmember fluids, where substantially faster reaction rates would be expected due to higher temperatures and reactant concentrations.

Elevated concentrations of other organically-derived aqueous species in these low-temperature mixed fluids provide compelling support for thermogenic CH_3SH production during mixing. As is evident at Guaymas, short-chain hydrocarbons and NH_4^+ are typically produced simultaneously during hydrothermal alteration of organic matter (35, 36, 39, 44). High CH_3SH concentrations in mixed fluids at Piccard, Von Damm, Rainbow and 9°50'N are associated with

210 excess NH_4^+ **(Fig. 3C and Fig. S1)** and, in some cases, low molecular weight hydrocarbon
211 (methane, ethane and propane) enrichments relative to conservative dilution of precursor
212 endmember fluids. For example, the low-temperature 'Hot Chimlet #1' vent at Piccard (see (32)
213 for images) is enriched by more than 25% in NH_4^+ and CH_4 relative to conservative dilution of
214 high-temperature endmember concentrations, and the low-temperature 'Ecurie' vent at Rainbow
215 is also enriched in both species **(Table S1)**. Ethane and propane are substantially enriched in
216 mixed fluids at Piccard (45), with concentrations as high as 90 nmol/kg ethane and 60 nmol/kg
217 propane in the mixed fluids 'Hot Chimlet #1' and 'Hot Chimlet #2', while associated endmember
218 fluids have much lower C_{2+} hydrocarbon concentrations (8-20 nmol/kg ethane, propane <10
219 nmol/kg (below detection)).
220 Abiotic N_2 reduction is unlikely to be responsible for the NH_4^+ enrichment in mixed
221 fluids, given that it is only thought to occur under high-temperature reaction zone conditions (44,
222 46). Admixing and abiotic reduction of seawater nitrate (NO_3^-) may be an alternate possible
223 source of NH_4^+ to mixed fluids, as experiments suggest metal catalysts (e.g. Fe-Ni alloy) could
224 mediate such reduction at low-temperatures (47), but this does not appear to be an important
225 process in low-temperature (~150°C) mixed fluids from other mafic-hosted hydrothermal systems
226 based on N-isotope measurements (42). Thermal degradation of dissolved organic nitrogen (DON)
227 from admixed ambient deep ocean seawater is also an unlikely source of NH_4^+. Some mixed
228 fluids are enriched in NH_4^+ above conservative endmember dilution by up to 4 μM (**Fig. 3C**),
229 exceeding what might reasonably be expected for entrainment and complete N release from
230 typical deep-ocean DON concentrations (<3 μM (48)). Although microbially-mediated nitrogen
231 transformations can increase the abundance of NH_4^+ in very low-temperature/diffuse fluids (42),
232 most large NH_4^+ and CH_3SH enrichments observed during this study (e.g. 'Hot Chimlet #1') are
233 in mixed fluids hotter than the 122°C limit for microbial life (49), suggesting that microbial
234 activity is not responsible for production of either NH_4^+ or CH_3SH.

It is widely proposed that the permeable and porous upper oceanic crust (Layer 2A), where mixing predominantly occurs, harbors microbial communities that constitute a deep biosphere (41-43). Given that CH_3SH in low-temperature mixed fluids is consistently associated with thermogenic indicators **(Fig. 3 and Fig. S1)** in systems free of sedimentary influence, we propose that entrainment and thermal alteration of microbial biomass, and/or associated dissolved organic matter (DOM), are responsible for production of CH_3SH within subsurface zones of mixing between high-temperature fluids with seawater. Previous observations of organic compounds derived from microbial biomass pyrolysis in low-temperature fluids support this possibility. Brault et al. (50) first described the presence of nonvolatile hydrocarbons in a diffuse (~15°C) and a high-temperature (>250°C) vent from 13°N, East Pacific Rise, and found strong enrichments of microbial lipid residues in the cooler vent. More recent work also suggests dissolved organic carbon (DOC) is enriched in low-temperature fluids relative to both endmember precursors and ambient seawater, for example, and correlates with microbial cell counts (51). While these observations could reflect active microbial processes, our results suggest higher temperature portions of subsurface mixing zones generate dissolved organic compounds through abiotic thermal degradation. Fluids in the temperature range presented here (e.g. 126 to 191°C) have rarely been reported, but provide key insights into processes occurring within crustal hydrothermal aquifers beyond the known 122°C (49) temperature limit of life.

The ubiquitous and uniformly low levels of CH_3SH (~10^{-8} M) in endmember fluids from unsedimented systems, despite the broad range of temperature, salinity and H_2 concentrations, may be a remnant of pyrolysis of trace organic matter at high temperatures. Brault et al. (50) noted minor quantities of thermally-mature hopanes in a hot fluid (>250°C) from 13°N, suggesting entrainment and rapid pyrolysis of biomass to a high extent of maturity occurs during fluid venting at the seafloor. Endmember fluids are also known to be depleted in dissolved organic carbon relative to ambient seawater (51), implying thermal decomposition. A thermogenic carbon source would provide an explanation for the presence of CH_3SH in fluids

with no thermodynamic drives to create it from CO_2. In a similar manner to the hotter endmember fluids at Guaymas Basin, consumption of CH_3SH by reaction **[2]** in high-temperature fluids could therefore represent the high maturity stage of much more limited organic matter pyrolysis during hydrothermal circulation or venting that produces insignificant changes in the abundance of major species like CH_4. Lost City endmember fluids, despite quite low vent temperatures (94–96°C, **Table S1**), are also consistent with this explanation. Several lines of evidence from the inorganic (52) and organic (53) compositions of endmember fluids there point to substantial conductive cooling and much higher temperatures (likely in excess of 250°C) in the subsurface reaction zone. Collectively, our data therefore imply the distribution of methanethiol in seafloor hydrothermal fluids is largely controlled by thermal maturation of pre-existing biological organic matter, with endmember and mixed vent fluids representing higher and lower thermal maturities, respectively.

Implications

Despite the diversity of geologic settings and potential catalytic minerals present in hydrothermal reaction zones, our results show no evidence for abiotic methanethiol synthesis from the inorganic precursors CO_2, H_2 and H_2S in modern hydrothermal fluids. This suggests that analogous hydrothermal systems on early Earth may not represent an abundant source of abiotic CH_3SH necessary for thioester production (4, 8, 12). The production of thermogenic organic compounds in crustal mixing zones, however, has numerous interesting biogeochemical implications for modern seafloor hydrothermal systems. Not only does widespread pyrolysis of subsurface organic matter provide further indirect support for a putative deep biosphere in unsedimented hydrothermal aquifers, it implies such carbon may be recycled and returned to cooler near-surface environments by subsurface mixing processes. Production of methylated organic compounds by subsurface pyrolysis raises diverse possibilities for microbial organotrophic metabolisms (e.g. methylotrophy) in hydrothermal systems traditionally considered to have limited available organic compounds. A predominance of thermogenic products in low-temperature fluids could support larger populations of organotrophic microbes in these mixing zones relative to those immediately surrounding high temperature vent structures, for example. Given that thiol functional groups are hypothesized to play a significant role in the complexation and delivery of hydrothermal trace metals (e.g. Fe and Cu) to the deep ocean (17-19), thermogenic production of organosulfur compounds with a high affinity for metals may constitute a key mechanism for this process in unsedimented hydrothermal systems.

ACKNOWLEDGMENTS.

We thank the captains and crews of the R/V Atlantis and R/V Roger Revelle and the crews of the HOV Alvin and the ROV Jason for their indispensable skills in sample collection. We are grateful to N. Pester and W. Seyfried for providing Mg and H2S data for TAG and Lost City. This research was supported by National Science Foundation Grants OCE-0702677, OCE-0549829, and OCE-1061863, and NASA Grant NNX-327 09AB75G (to J.S.S.); and by funding from the Woods Hole Oceanographic Institution Deep Ocean Exploration Institute, InterRidge, and the Deutsche Forschungsgemeinschaft Research Center/Cluster of Excellence MARUM "The Ocean in the Earth System" (E.P.R.).

Materials and Methods

Sample Collection and Analysis

All fluid samples were collected using isobaric gas-tight (IGT) samplers (27) during cruises to the Mid-Atlantic Ridge, Guaymas Basin and East Pacific Rise in 2008 and Mid-Cayman Rise in 2012, using either ROV *Jason* or HOV *Alvin*. In most cases a minimum of two IGT samples were taken from each vent. Reported vent temperatures are the maximum measured in real-time during fluid collection (27).

Dissolved CH_3SH concentrations were determined at sea upon sampler recovery by purge-and-trap gas chromatography (GC) with flame ionization detection (FID). FID, unlike sulfur-specific detection, is insensitive to the extremely high H_2S concentrations in vent fluids. Gas-tight fluid aliquots (<4mL) were acidified with ~1mL of 25wt.% phosphoric acid and CH_3SH was sparged with He gas (30mL/min for 10 min) and cryo-focused on an *n*-octane-coated silica trap (-78°C), then thermally desorbed (145°C) directly onto a Carbograph 1SC packed GC column (30mL/min He, 40°C isothermal). To limit potential losses of gaseous CH_3SH during sparging (54, 55), de-activated glass and PTFE tubing were used wherever possible in the purge-and-trap system. Sparging was assumed to be quantitative given the long sparge time and volatility of CH_3SH, and re-sparging tests on samples revealed no significant evidence of incomplete removal. Before calibration and between samples, the trap was heated at >145°C with He flowing (30mL/min) for a minimum of 10 minutes to completely eliminate carryover of any residual CH_3SH remaining in the trap (typically <1%) from previous analyses. In almost all cases, resulting CH_3SH concentration from separate discrete samplers of the same vent yield mixing lines between bottom seawater (no detectable CH_3SH) and a hydrothermal endmember or mixed fluid composition when plotted against Mg (see ***SI Text, Section 1*** for further details). This not only indicates that methanethiol is conservative with respect to accidental seawater entrainment during sample collection, but that any losses or additions of CH_3SH due to the analytical method are not significant. Reported uncertainties (2s) for CH_3SH **(Table S1)** are the larger of either the error of reproducibility or the error of the commercial gas standard used (±5%).

H_2 and CO were analyzed at sea by a headspace extraction GC technique, using thermal conductivity (TCD) and helium ionization (HID) detection, respectively (37, 39). H_2S (total dissolved, ΣH_2S) was determined either gravimetrically by precipitation as Ag_2S (56), or at sea by electrochemical (28, 33) or iodimetric titration. pH(25°C) was determined at sea by electrode (28, 33, 56). Aliquots for dissolved inorganic carbon (ΣCO_2, abbreviated as CO_2), CH_4 and C_{2+} hydrocarbons were stored in evacuated glass serum vials (poisoned with $HgCl_2$) for headspace

gas GC analysis (28, 56). Cl was determined by ion chromatography (IC, ±5% (56)) or electrochemical titration (±0.5%, (28, 33)) and Mg by either IC, ICP-MS or ICP-OES (28, 33, 56, 57). NH_4^+ was determined either by flow injection analysis (58) for unsedimented systems or IC (Guaymas Basin), with reported errors representing the larger or either error of reproducibility (2s) or the typical ±5% reproducibility of prepared standards. Analytical uncertainties (2s) are ±0.05 for pH(25°C), ±10% for H_2S, CO, H_2 and C_{2+} hydrocarbon concentrations, and ±5% for Mg, ΣCO_2 and CH_4 concentrations (28, 39, 56).

References

1. Corliss JB, Baross JA, & Hoffman SE (1981) An hypothesis concerning the relationship between submarine hot springs and the origin of life on Earth: Proceedings, 26th International Geological Congress, Geology of Oceans Symposium, Paris, July 7-17, 1980. *Oceanologica Acta* 4(Supplement):59-69.
2. Baross JA & Hoffman SE (1985) Submarine hydrothermal vents and associated gradient environments as sites for the origin and evolution of life. *Orig. Life Evol. Biosph.* 15(4):327-345.
3. Holm N (1992) Why are hydrothermal systems proposed as plausible environments for the origin of life? *Orig. Life Evol. Biosph.* 22(1-4):5-14.
4. Martin W, Baross J, Kelley D, & Russell MJ (2008) Hydrothermal vents and the origin of life. *Nature Rev. Microbiol.* 6(11):805-814.
5. Sousa FL*, et al.* (2013) Early bioenergetic evolution. *Phil. Trans. R. Soc. B* 368(1622):20130088.
6. Kelley DS, Baross JA, & Delaney JR (2002) Volcanoes, fluids, and life at mid-ocean ridge spreading centers. *Annu. Rev. Earth Planet. Sci.* 30:385-491.
7. McCollom TM & Seewald JS (2007) Abiotic synthesis of organic compounds in deep-sea hydrothermal environments. *Chem. Rev.* 107:382-401.
8. Huber C & Wachtershauser G (1997) Activated acetic acid by carbon fixation on (Fe,Ni)S under primordial conditions. *Science* 276(5310):245-247.
9. Huber C & Wachtershauser G (1998) Peptides by activation of amino acids with CO on (Ni,Fe)S surfaces: Implications for the origin of life. *Science* 281(5377):670-672.
10. Cody GD*, et al.* (2000) Primordial carbonylated iron-sulfur compounds and the synthesis of pyruvate. *Science* 289(5483):1337-1340.
11. Huber C & Wachterschauser G (2006) α-Hydroxy and α-amino acids under possible Hadean, volcanic origin-of-life conditions. *Science* 314(5799):630-632.
12. Russell MJ & Hall AJ (2006) The onset and early evolution of life. *Evolution of Early Earth's Atmosphere, Hydrosphere, and Biosphere - Constraints from Ore Deposits: Geological Society of America Memoir 198*, eds Kesler SE & Ohmoto H, pp 1-32.
13. Martin W & Russell MJ (2006) Review: On the origin of biochemistry at an alkaline hydrothermal vent. *Phil. Trans. R. Soc. B*: URL: http://dx.doi.org/1010.1098/rstb.2006.1881.
14. Novikov Y & Copley SD (2013) Reactivity landscape of pyruvate under simulated hydrothermal vent conditions. *Proc. Nat. Acad. Sci. USA* 110(33):13283-13288.

15. Rogers KL & Schulte MD (2012) Organic sulfur metabolisms in hydrothermal environments. *Geobiology*.
16. Lomans BP*, et al.* (1997) Formation of dimethyl sulfide and methanethiol in anoxic freshwater sediments. *Appl. Environ. Microbiol.* 63(12):4741-4747.
17. Sander SG, Koschinsky A, Massoth G, Stott M, & Hunter KA (2007) Organic complexation of copper in deep-sea hydrothermal vent systems. *Envir. Chem.* 4(2):81-89.
18. Sander SG & Koschinsky A (2011) Metal flux from hydrothermal vents increased by organic complexation. *Nature Geosci.* 4(3):145-150.
19. Toner BM*, et al.* (2009) Preservation of iron(II) by carbon-rich matrices in a hydrothermal plume. *Nature Geosci.* 2(3):197-201.
20. Heinen W & Lauwers AM (1996) Organic sulfur compounds resulting from the interaction of iron sulfide, hydrogen sulfide and carbon dioxide in an anaerobic aqueous environment. *Orig. Life Evol. Biosph.* 26(2):131-150.
21. Loison A, Dubant S, Adam P, & Albrecht P (2010) Elucidation of an iterative process of carbon–carbon bond formation of prebiotic significance. *Astrobiology* 10(10):973-988.
22. Schulte MD & Rogers KL (2004) Thiols in hydrothermal solution: standard partial molal properties and their role in the organic geochemistry of hydrothermal environments. *Geochim. Cosmochim. Acta* 68(5):1087-1097.
23. Charlou JL*, et al.* (2010) High Production and Fluxes of H_2 and CH_4 and Evidence of Abiotic Hydrocarbon Synthesis by Serpentinzation in Ultramafic-Hosted Hydrothermal Systems on the Mid-Atlantic Ridge. *Diversity of Hydrothermal Systems on Slow Spreading Ocean Ridges,* AGU Monograph, eds Rona P, Devey CW, Dyment J, & Murton BJ (American Geophysical Union), Vol 188, pp 265-296.
24. Proskurowski G*, et al.* (2008) Abiogenic hydrocarbon production at Lost City hydrothermal field. *Science* 319(5863):604-607.
25. Lang SQ, Butterfield DA, Schulte M, Kelley DS, & Lilley MD (2010) Elevated concentrations of formate, acetate and dissolved organic carbon found at the Lost City hydrothermal field. *Geochim. Cosmochim. Acta* 74(3):941-952.
26. McCollom TM (2008) Observational, Experimental, and Theoretical Constraints on Carbon Cycling in Mid-Ocean Ridge Hydrothermal Systems. *The Subseafloor Biosphere at Mid-Ocean Ridges,* AGU Monograph, eds Wilcock WSD, DeLong EF, Kelley DS, Baross JA, & Cary SC (American Geophysical Union), Vol 144, pp 193-213.
27. Seewald JS, Doherty KW, Hammar TR, & Liberatore SP (2002) A new gas-tight isobaric sampler for hydrothermal fluids. *Deep-Sea Res. Pt. I* 49(1):189-196.

28. Pester NJ, *et al.* (2012) Subseafloor phase equilibria in high-temperature hydrothermal fluids of the Lucky Strike Seamount (Mid-Atlantic Ridge, 37°17'N). *Geochim. Cosmochim. Acta* 90:303-322.
29. Foustoukos DI & Seyfried WE (2005) Redox and pH constraints in the subseafloor root zone of the TAG hydrothermal system, 26° N Mid-Atlantic Ridge. *Earth Planet. Sci. Lett.* 235(3-4):497-510.
30. Proskurowski G, Lilley MD, & Olson EJ (2008) Stable isotopic evidence in support of active microbial methane cycling in low-temperature diffuse flow vents at 9°50'N East Pacific Rise. *Geochim. Cosmochim. Acta* 72(8):2005-2023.
31. German CR, *et al.* (2010) Diverse styles of submarine venting on the ultraslow spreading Mid-Cayman Rise. *Proc. Nat. Acad. Sci. USA* 107(32):14020-14025.
32. Kinsey, J.C & German, C.R. (2013) Sustained volcanically-hosted venting at ultraslow ridges: Piccard Hydrothermal Field, Mid-Cayman Rise. *Earth Planet. Sci. Lett.* 380:162–168.
33. Seyfried WE, Pester NJ, Ding K, & Rough M (2011) Vent fluid chemistry of the Rainbow hydrothermal system (36°N, MAR): Phase equilibria and in situ pH controls on subseafloor alteration processes. *Geochim. Cosmochim. Acta* 75(6):1574-1593.
34. Connelly DP, *et al.* (2012) Hydrothermal vent fields and chemosynthetic biota on the world's deepest seafloor spreading centre. *Nature Communications* 3:620.
35. Von Damm KL, Edmond JM, Measures CI, & Grant B (1985) Chemistry of submarine hydrothermal solutions at Guaymas Basin, Gulf of California. *Geochim. Cosmochim. Acta* 49(11):2221-2237.
36. Welhan JA & Lupton J (1987) Light hydrocarbon gases in Guaymas Basin hydrothermal fluids: Thermogenic versus abiogenic origin. *AAPG Bull.* 71(2):215-223.
37. Seewald JS, Zolotov MY, & McCollom T (2006) Experimental investigation of single carbon compounds under hydrothermal conditions. *Geochim. Cosmochim. Acta* 70(2):446-460.
38. Kawka OE & Simoneit BRT (1987) Survey of hydrothermally-generated petroleums from the Guaymas Basin spreading center. *Org. Geochem.* 11(4):311-328.
39. Cruse AM & Seewald JS (2006) Geochemistry of low-molecular weight hydrocarbons in hydrothermal fluids from Middle Valley, northern Juan de Fuca Ridge. *Geochim. Cosmochim. Acta* 70(8):2073-2092.

40. Krein EB (1993) Organic sulfur in the geosphere: analysis, structures and chemical processes. *Supplement S: The chemistry of Sulphur-containing functional groups*, eds Patai S & Rappoport Z (Wiley), pp 975-1032.
41. Summit M (2001) Special Feature: A novel microbial habitat in the mid-ocean ridge subseafloor. *Proc. Nat. Acad. Sci. USA* 98(5):2158-2163.
42. Bourbonnais A, Lehmann MF, Butterfield DA, & Juniper SK (2012) Subseafloor nitrogen transformations in diffuse hydrothermal vent fluids of the Juan de Fuca Ridge evidenced by the isotopic composition of nitrate and ammonium. *Geochem. Geophys. Geosys.* 13(1): Q02T01, doi:10.1029/2011GC003863
43. Orcutt BN, Sylvan JB, Knab NJ, & Edwards KJ (2011) Microbial Ecology of the Dark Ocean above, at, and below the Seafloor. *Microbiol. Mol. Biol. Rev.* 75(2):361-422.
44. Lilley MD*, et al.* (1993) Anomalous CH_4 and NH_4^+ concentrations at an unsedimented mid-ocean-ridge hydrothermal system. *Nature* 364(6432):45-47.
45. McDermott JM*, et al.* (2012) Abundance of volatile and organic species in intermediate temperature fluids from the Von Damm and Piccard deep sea hydrothermal fields, Mid-Cayman Rise. *Paper presented at the AGU Fall Meeting, 3-7 December 2012 (abstract OS22B–07)*.
46. Brandes JA, Hazen RM, & Yoder HS (2008) Inorganic Nitrogen Reduction and Stability under Simulated Hydrothermal Conditions. *Astrobiology* 8(6):1113-1126.
47. Smirnov A, Hausner D, Laffers R, Strongin DR, & Schoonen MAA (2008) Abiotic ammonium formation in the presence of Ni-Fe metals and alloys and its implications for the Hadean nitrogen cycle. *Geochem. T.* 9(1):5.
48. Wong CS, Yu Z, Waser NAD, Whitney FA, & Johnson WK (2002) Seasonal changes in the distribution of dissolved organic nitrogen in coastal and open-ocean waters in the North East Pacific: sources and sinks. *Deep-Sea Res. Pt. II* 49(24-25):5759-5773.
49. Takai K*, et al.* (2008) Cell proliferation at 122°C and isotopically heavy CH_4 production by a hyperthermophilic methanogen under high-pressure cultivation. *Proc. Nat. Acad. Sci. USA* 105(31):10949-10954.
50. Brault M, Simoneit BRT, Marty JC, & Saliot A (1988) Hydrocarbons in waters and particulate material from hydrothermal environments at the East Pacific Rise, 13°N. *Org. Geochem.* 12(3):209-219.
51. Lang SQ, Butterfield DA, Lilley MD, Johnson HP, & Hedges JI (2006) Dissolved organic carbon in ridge-axis and ridge-flank hydrothermal systems. *Geochim. Cosmochim. Acta* 70(15):3830-3842.

52. Foustoukos, D.I., Savov, I.P., and Janecky, D.R. (2008) Chemical and isotopic constraints on water/rock interactions at the Lost City hydrothermal field, 30°N Mid-Atlantic Ridge. *Geochimica et Cosmochimica Acta* 72: 5457-5474.

53. Reeves EP, Seewald JS, and Sylva SP (2012) Hydrogen isotope exchange between *n*-alkanes and water under hydrothermal conditions. *Geochim. Cosmochim. Acta* 77: 582-599.

54. Simo R (1998) Trace chromatographic analysis of dimethyl sulfoxide and related methylated sulfur compounds in natural waters. *J. Chrom. A* 807(2):151-164.

55. Wardencki W (1998) Problems with the determination of environmental sulphur compounds by gas chromatography. *J. Chrom. A* 793(1):1-19.

56. Reeves EP*, et al.* (2011) Geochemistry of hydrothermal fluids from the PACMANUS, Northeast Pual and Vienna Woods hydrothermal fields, Manus Basin, Papua New Guinea. *Geochim. Cosmochim. Acta* 75:1088–1123.

57. Craddock PR*, et al.* (2010) Rare earth element abundances in hydrothermal fluids from the Manus Basin, Papua New Guinea: Indicators of sub-seafloor hydrothermal processes in back-arc basins. *Geochim. Cosmochim. Acta* 74:5494-5513.

58. Hall PO & Aller RC (1992) Rapid, small-volume, flow injection analysis for ΣCO_2 and NH_4^+ in marine and fresh-waters. *Limnol. Oceanogr.* 37(5):1113-1119.

494 **Figure Captions**

495

496 **Fig. 1.** Plot of predicted concentrations ($m_{\text{Methanethiol}}$, mol/kg H_2O) of methanethiol (CH_3SH) in
497 metastable equilibrium with CO_2, H_2 and H_2S according to reaction **[1]** versus observed
498 concentrations ($M_{\text{Methanethiol}}$, mol/L fluid) for endmember (*black symbols*) and mixed (*color*
499 *symbols*) hydrothermal fluids emanating from unsedimented mafic and ultramafic geologic
500 settings, with respective ranges of dissolved H_2 concentration shown in the legend (**see *SI Text,***
501 ***Sections 1 and 4*, for further details**). Predicted values were calculated assuming ideal behavior
502 of neutral aqueous species. Observed concentrations of CH_3SH in fluids with low dissolved H_2
503 are in excess of predicted values, and, conversely, are below predicted values in high-H_2 fluids.
504 Highest observed concentrations of CH_3SH are in low-temperature mixed fluids at Piccard, Von
505 Damm and Rainbow (see text). The apparent trend of predicted and observed values at Piccard is
506 a consequence of co-varying H_2 and CH_3SH during subsurface mixing with seawater.

507

508 **Fig. 2.** Plots of measured concentrations of chloride (Cl, **A**), methanethiol (CH_3SH, **B**) and
509 ammonium (NH_4^+, **C**) versus Mg in Guaymas Basin vent fluid samples, showing CH_3SH and
510 NH_4^+ production. Mg is used as an index of mixing between seawater and vent fluid (**see *SI Text,***
511 ***Section 1* for further details**). Cooler endmember fluids (Theme Park, Cathedral Hill, Sulfide
512 Spires, *solid symbols*) from areas of hydrothermal petroleum expulsion have higher CH_3SH
513 concentrations and lower $C_1/(C_2+C_3)$ ratios (<60) than hotter fluids from large flange structures
514 (>124; Toadstool, Rebecca's Roost, *open symbols*), implying thermal maturity differences (see
515 text). Cl **(A)** suggests a common source endmember, and while all fluids interacted with
516 sedimentary organic matter under hydrothermal conditions, yielding elevated NH_4^+ **(C)**, CH_3SH
517 **(B)** and C_{2+} hydrocarbons have likely decomposed to CH_4 at the higher thermal stress of the
518 hotter fluids. Uncertainties (2s) not shown are smaller than data symbols.

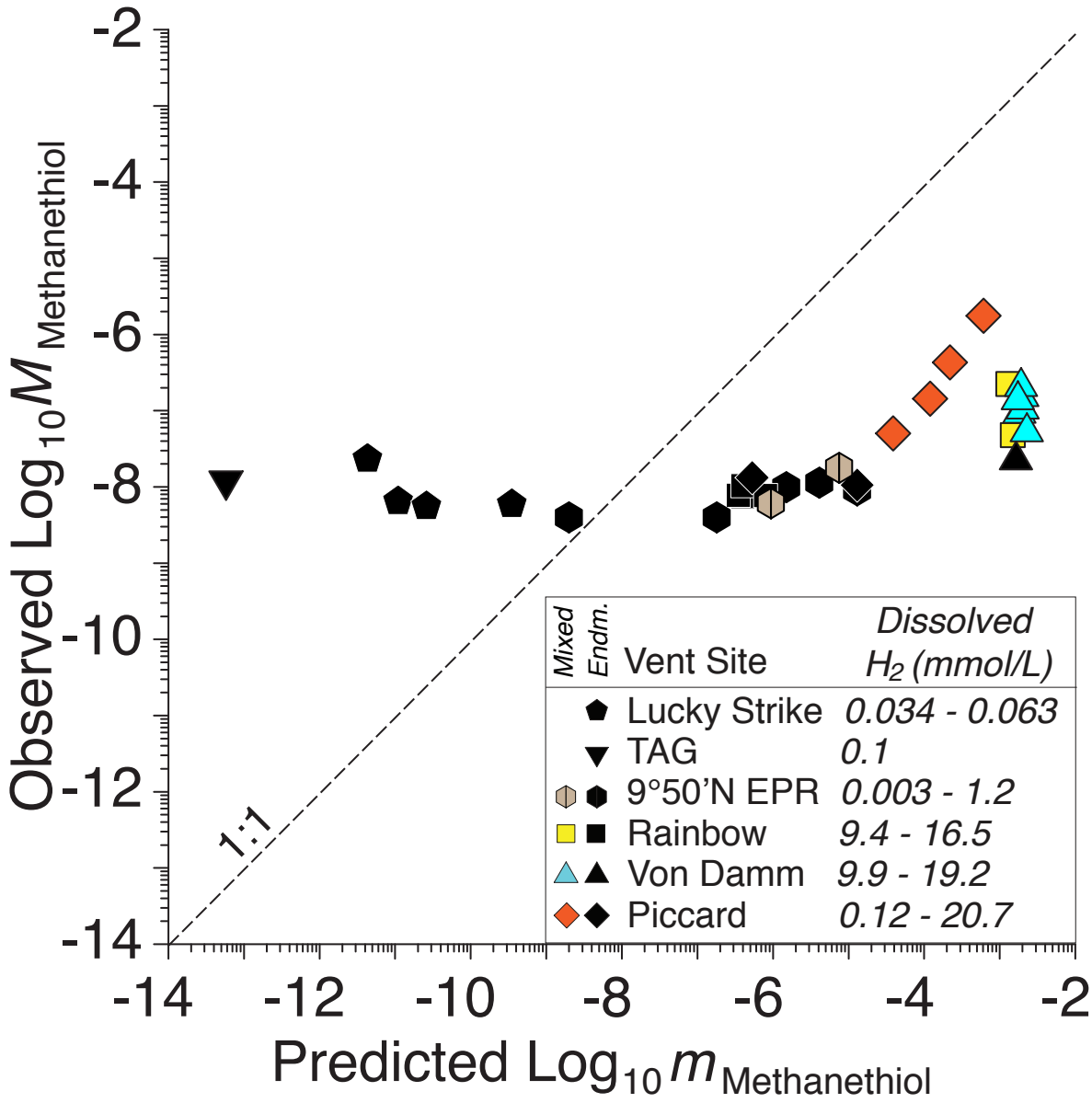
-2
-4
-6
-8
-10
-12
-14
Observed Log10 M Methanethiol
-14
-12
-10
-8
-6
-4
-2
Predicted Log10 m Methanethiol
1:1
Mixed
Endm.
Vent Site
Dissolved H2 (mmol/L)
Lucky Strike 0.034 - 0.063
TAG 0.1
9°50'N EPR 0.003 - 1.2
Rainbow 9.4 - 16.5
Von Damm 9.9 - 19.2
Piccard 0.12 - 20.7

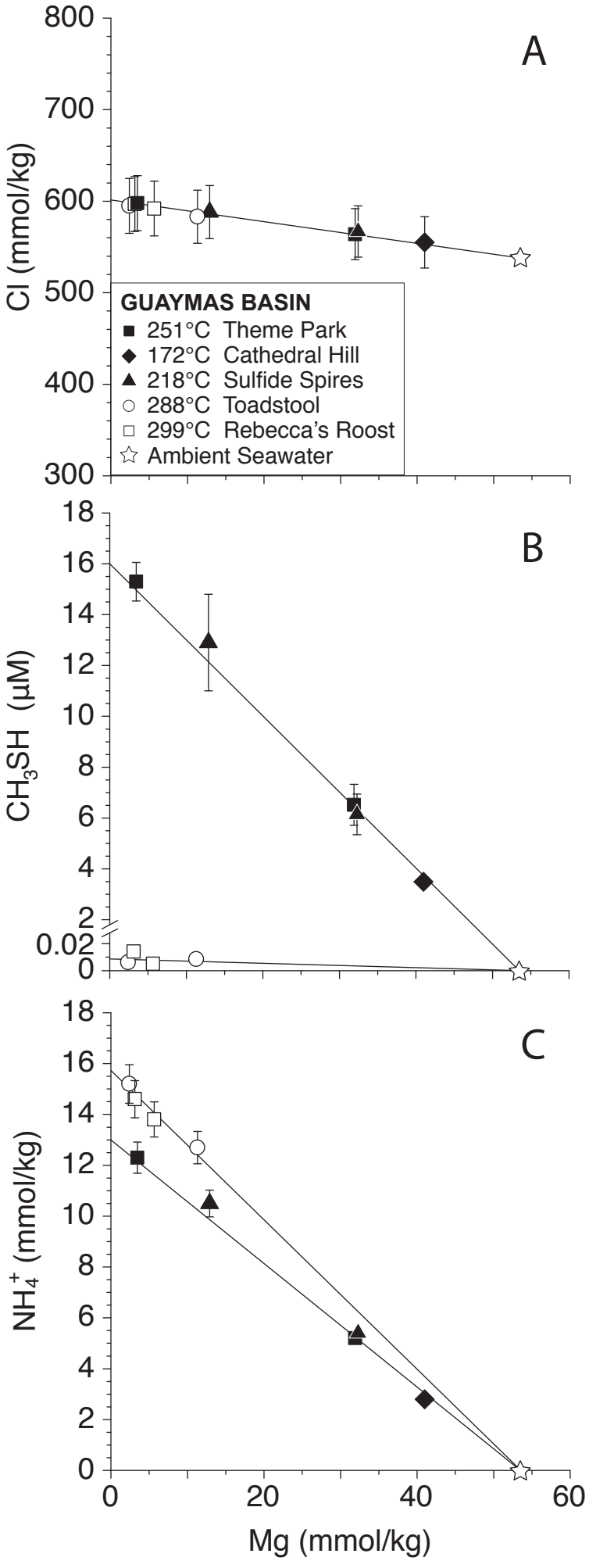
A
B
C
Cl (mmol/kg)
CH3SH (μM)
NH4+ (mmol/kg)
Mg (mmol/kg)
GUAYMAS BASIN
251°C Theme Park
172°C Cathedral Hill
218°C Sulfide Spires
288°C Toadstool
299°C Rebecca's Roost
Ambient Seawater

519 **Fig. 3.** Plots of measured concentrations of chloride (Cl, **A**), methanethiol (CH_3SH, **B**) and
520 ammonium (NH_4^+, **C**) versus Mg in fluid samples from three unsedimented hydrothermal vent
521 fields. Mg is used as an index of mixing between seawater and vent fluid (**see *SI Text, Section 1***
522 ***for further details***). Low Mg samples from high-temperature endmember fluids (*open symbols*),
523 and higher Mg samples from low-temperature fluids (*half filled/solid symbols*) at each field all lie
524 on common mixing lines with respect to Cl, indicating single common source fluids at each site.
525 At all vent fields, the higher Mg, low-temperature fluids formed by predominantly subsurface
526 mixing with seawater (*dashed lines*) are enriched in CH_3SH and NH_4^+ (and low molecular weight
527 alkanes, see text) relative to conservative dilution of endmember fluids (*solid lines*) with seawater.
528 Uncertainties (2s) not shown are smaller than the data symbols.

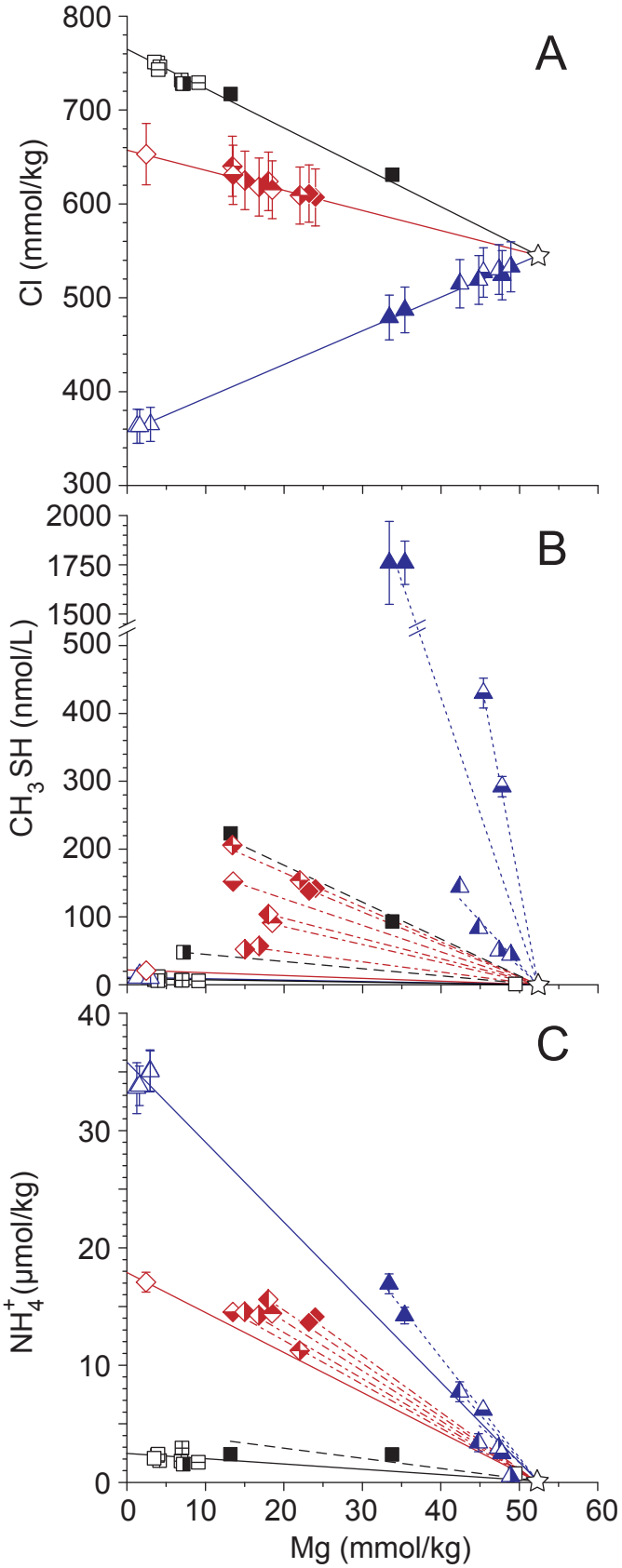

RAINBOW VENT FIELD	
PP27	350°C
Stylo 1	367°C
CMSP&P	365°C
Stylo 2	364°C
Ecurie	191°C
Mussel Beach	180°C
Bottom Seawater	

VON DAMM VENT FIELD	
East Summit	226°C
Arrow Loop #1	134°C
White Castle	151°C
Ginger Castle	128°C
Ravelin #1	145°C
Ravelin #2	116°C
West Summit	126°C

PICCARD VENT FIELD	
Beebe 3	397°C
Beebe Woods	354°C

Hot Chimlet #1	149°C
Hot Chimlet #2	95°C
Shrimp Gulley	45°C
N. Shrimp Gulley	111°C

Supporting Information

Reeves et al.

SI Text

1. 'Endmember' and 'mixed' vent fluid compositions

Based on their compositions and temperatures, we classify fluids into two categories, namely undiluted 'endmember' fluids, which have undergone no mixing in the crustal subsurface prior to venting at the seafloor, and 'mixed' fluids which appear to have been diluted and cooled with a seawater-like fluid prior to venting. Our calculations also take into account mixing of hydrothermal fluids with seawater during sample collection. Endmember fluid compositions referred to in **Table S1** are assumed to be devoid of Mg due to near-quantitative Mg removal from seawater during high-temperature water/rock interactions at reaction zone conditions (1-3), and are calculated as such by extrapolating measured species concentrations to zero Mg concentration using a linear regression forced through seawater (4). When endmember fluids mix with cooler seawater-like fluids during upflow through crustal aquifers, however, the resulting mixed fluids vent with Mg concentrations that lie between the endmember fluids and seawater (5). These fluids are readily identifiable by near-identical Mg concentrations in replicate samples of the same fluid, which are unlikely to be the result of accidental sampling-related seawater admixing, and temperatures lower than nearby endmember fluids **(Table S1)**. For non-conservative species, a zero Mg endmember calculated from a mixed fluid composition has no physical meaning (5). In the context of thermodynamic predictions, compositions of mixed fluids are therefore assumed to be that of the lowest measured Mg concentration, which best resembles the mixture venting at the seafloor. We arbitrarily define those fluids with similar Mg concentrations greater than 10 mmol/kg in duplicate IGT samples as 'mixed'. In fluids with less than 10 mmol/kg, compositions so closely resemble endmembers that zero Mg compositions are used. While this approach potentially neglects minor mixing, extrapolation to zero Mg compositions does not significantly alter our thermodynamic calculations or conclusions.

In cases where only one successful sample was taken, or where replicate samples yielded dissimilar Mg due to accidental seawater entrainment, the degree of purely subsurface mixing is unclear. Where replicate samples provide evidence for high Mg fluids due to subsurface mixing within a vent field (e.g. Piccard, Von Damm, 9°50'N), however, we reasonably assume that other low temperature fluids with high Mg are also 'mixed' in the subsurface. At the Rainbow site, the evidence that mixing alone formed low-temperature fluids (180–191°C) is unclear. Therefore, while we use lowest Mg compositions and measured temperatures in thermodynamic calculations,

we cannot preclude the effects of conductive cooling there. Regardless, the difference between model predictions at lowest Mg and calculated endmember compositions would not alter our conclusions regarding metastable equilibrium.

2. Assessment of metastable equilibrium using chemical affinities

Assuming the concentrations of species in either endmember and mixed fluids suffice to approximate activities for dissolved gases (i.e. activity coefficients equal 1), the equilibrium state of reactions (e.g. **[1]** and **[2]**) can be evaluated at the temperature and pressure conditions of venting by calculating the chemical affinity (A) from equation **[S1]**:

$$A = -\Delta_r G = -RT \ln (Q_r / K_{eq}) \qquad \textbf{[S1]}$$

Where R is the universal gas constant, T is the temperature of the vent fluid in Kelvin, Q_r is the reaction quotient and K_{eq} is the equilibrium constant at T and seafloor pressure. Calculated affinities of 0±5 kJ/mol are typically assumed to be representative of equilibrium, based on estimated errors in derived $\Delta_r G°$ values (6, 7).

3. Widespread CO_2-H_2-CO equilibrium in unsedimented systems

The data presented in **Table S1** confirm the findings of Seewald *et al.*(8) that CO concentrations measured in hydrothermal fluids emanating from unsedimented systems are strictly regulated by equilibrium according to the water-gas shift reaction:

$$CO_{2(aq)} + H_{2(aq)} \leftrightarrow CO_{(aq)} + H_2O_{(l)} \qquad \textbf{[S2]}$$

Calculated affinities for reaction **[S2]** at the conditions and compositions of vent fluids from the unsedimented systems Rainbow (-0.09 to +5.7 kJ/mol) and 9°50'N (+0.9 to +4.7 kJ/mol) are all therefore close to or within reasonable error of equilibrium. In H_2-poor fluids where CO was not detectable **(Table S1)**, reaction **[S2]** predicts concentrations below the detection limit of the analytical method. Guaymas Basin fluids (172–218°C) heavily influenced by thermal alteration of organic matter provide the only deviation (-14.3 to -19.3kJ/mol) from near-equilibrium affinities, where high CO concentrations (26–92μM) are in excess of equilibrium predictions according to reaction **[S2]** (see discussion in text).

4. Thermodynamic prediction of metastable CH_3SH abundances

The abundance of aqueous CH_3SH at metastable equilibrium according to reaction **[1]** was predicted for each vent fluid using the REACT module of the computer code Geochemist's Workbench™ **(Fig.1 and Table S1)**. For all calculations, the 50 MPa database of Amend et al.(9) was used, which includes thermodynamic data for aqueous CH_3SH at elevated temperatures (10).

The effect of pressure on model predictions is negligible. Predictions cannot be reliably made for high pH Lost City fluids, due to the lack of thermodynamic data for dissociation of CH_3SH to form methanethiolate (CH_3S^-) at vent conditions, as well as large uncertainties in the estimation of extremely low endmember DIC concentrations (11). Predictions are also not made for Guaymas Basin fluids, as disequilibrium between CO and CO_2 (see text) invalidates the model assumptions outlined below. Respective ΣCO_2, H_2S and H_2 concentrations, and pH(25°C) of either zero Mg endmember or mixed fluid compositions were used as initial mass balance constraints and respeciated from 25°C to vent temperatures using endmember or mixed fluid Cl concentrations (charge balanced with equivalent Na), while suppressing formation of CH_4 and any C_{2+} organic compounds or mineral phases. Activity coefficients of 1 were assumed for all neutral species in the model.

In addition to using ΣCO_2, H_2S and H_2 to conserve mass, the speciation model also allows metastable equilibrium between single carbon compounds (formic acid (HCOOH), formate ($HCOO^-$), carbon monoxide (CO), formaldehyde (CH_2O) and methanol (CH_3OH)) and CO_2 and H_2, in addition to carbonate equilibria. It is therefore identical to that of Seewald et al.(8) except that it additionally considers CH_3SH formation and H_2S speciation. Volatile species in the model whose concentrations were determined at sea (CH_3SH, H_2, H_2S) necessarily have units of molarity (i.e. mol/L fluid measured at room temperature). As for ΣCO_2 (mmol/kg fluid), these units can all be assumed to be comparable to corresponding units of molality (mol/kg solvent) calculated by the model. For fluids of the salinities presented in this study, explicitly correcting values would only result in a <2% difference (12), which is smaller than analytical uncertainties.

Fig. S1.

Plots of measured concentrations of chloride (Cl, **A**), methanethiol (CH_3SH, **B**) and ammonium (NH_4^+, **C**) versus Mg in fluid samples 9°50'N East Pacific Rise hydrothermal fluids, showing CH_3SH and NH_4^+ production there. Various 'L Vent' fluids shown refer to separate orifices on the L Vent structure described previously (13), with 'L Vent Fissure' being a nearby low-temperature vent sharing the same endmember precursor. 'Crab Spa' is a low-temperature vent located near 'Tica', which is its likely endmember parent. Both low-temperature mixed fluids (*open symbols*) have elevated CH_3SH and NH_4^+ relative to conservative dilution of their respective source fluids. Despite wide variations in Cl at this site (e.g. L Vent versus Trick or Treat vent), CH_3SH does not vary inversely with Cl as is typical for other volatile species, suggesting that it must form subsequent to phase separation. Uncertainties (2s) not shown are smaller than data symbols.

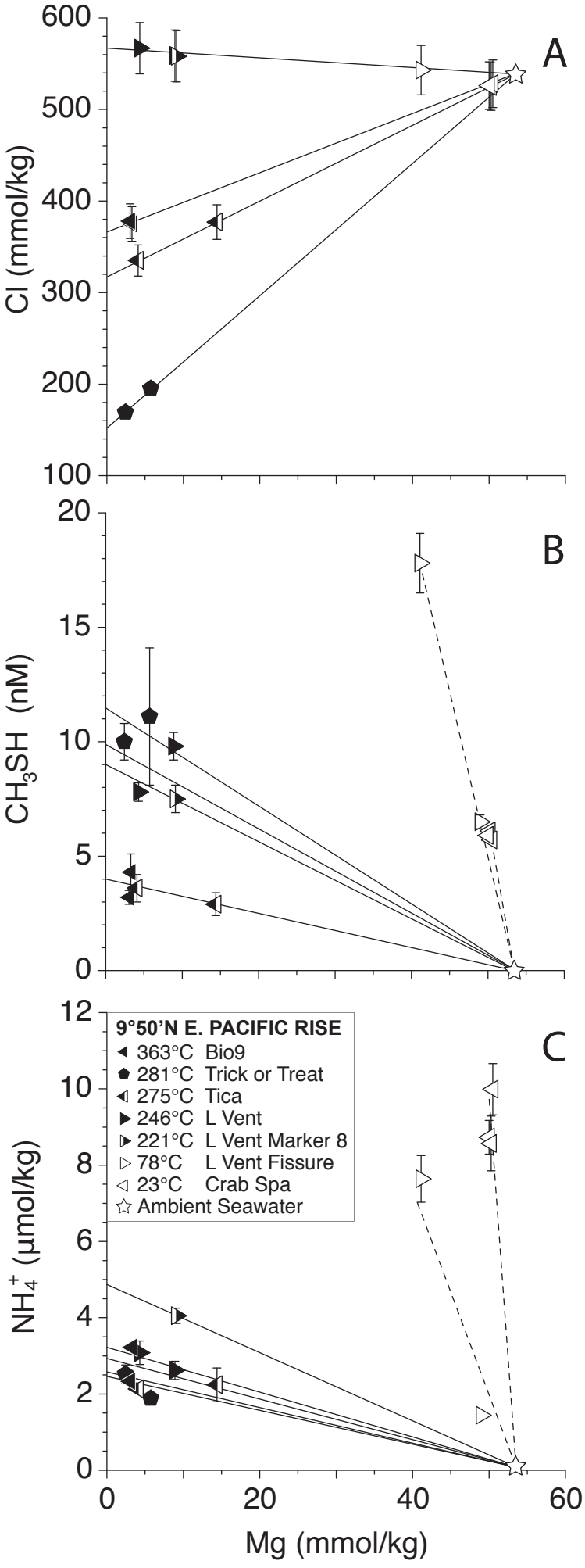
A
B
C
Cl (mmol/kg)
CH_3SH (nM)
NH_4^+ (µmol/kg)
Mg (mmol/kg)
600
500
400
300
200
100
20
15
10
5
0
12
10
8
6
4
2
0
0
20
40
60
9°50'N E. PACIFIC RISE
363°C Bio9
281°C Trick or Treat
275°C Tica
246°C L Vent
221°C L Vent Marker 8
78°C L Vent Fissure
23°C Crab Spa
Ambient Seawater

Table S1.

Measured and calculated concentrations of dissolved species in hydrothermal fluids

Complete data table containing measured temperatures, pH(25°C) and concentrations of Mg, Cl, H_2, H_2S, ΣCO_2, CO, CH_4, NH_4^+, CH_3SH (and predicted CH_3SH), and corresponding endmember or lowest Mg values for species used in the thermodynamic model (*bold entries*). Data for temperature, pH(25°C), Mg, Cl and CH_4 for Rainbow and Lucky Strike IGT samples shown here have been published previously (14, 15). A bottom seawater NH_4^+ concentration of 0.1 μmol/kg is assumed based on typical values (e.g. (16)).

Table S1 notes and abbreviations:

Only maximum temperatures measured during sampling an individual vent are reported.

Units: **mm** = mmol/kg fluid ; **mM** = mmol/L fluid ; **μm** = μmol/kg fluid; **μM** =μmol/L fluid; **nM** = nmol/L fluid; **nmolal** = nmol/kg H_2O

Methanethiol and NH_4^+ errors (2s) are the greater of either error of reproducibility or 5% analytical error of standard and (*n*) refers to the number of CH_3SH measurements per IGT.

‡ **Bottom seawater CH_3SH** was below detection in an IGT sample of ambient bottom seawater from the East Pacific Rise and is therefore assumed absent

nd = not determined,

***** = Model predictions not possible for Lost City and Guaymas Basin **(see *SI Text, Section 4*)**

BD = below detection

§ Lost City and TAG chloride data are not available for 2008. Given the temporal stability of the system (17), the most recent Cl endmember (669 mmol/kg) was used for TAG endmember modeling.

Table S1. Measured and calculated endmember concentrations of dissolved species

SITE (depth, location) Vent (Max. temp. °C)	Sample	Mg (mm)	Cl (mm)	pH (25°C)	H_2 (mM)	H_2S (mM)	ΣCO_2 (mm)	CO (µM)	CH_4 (mM)	NH_4^+ (µm (±2s))	Measured CH_3SH (nM (±2s, *n*))	Predicted CH_3SH nmolal
RAINBOW (2300m, 36°13.80'N–33°54.15'W)												
Endmember Fluids												
PP27/Exo2/Padraig/Termitiere (350°C)	J2-353-IGT-3	6.90	732	3.35	10.7	2.7	19.6	4.5	1.73	1.8(±0.28)	6.7(±0.3, *1*)	-
	J2-353-CGT-R	7.05	728	3.59	10.6	3.0	17.8	4.4	1.76	2.9(±0.15)	6.5(±0.3, *1*)	-
	Endmember	**0**	**758**	**3.35**	**12.3**	**3.3**	**21.3**	**5.1**	**2.01**	2.7	**7.7**	**$8.0x10^2$**
Stylo 1 (367°C)	J2-354-IGT-5	4.17	746	3.31	15.0	1.9	23.4	6.6	1.95	1.9(±0.21)	7.6(±0.8, *4*)	-
	J2-354-CGT-B	3.92	750	3.39	14.8	2.3	22.3	6.8	1.93	2.3(±0.23)	6.1(±0.9, *3*)	-
	Endmember	**0**	**765**	**3.31**	**16.1**	**2.3**	**24.6**	**7.2**	**2.10**	2.3	**7.4**	**$4.0x10^2$**
CMSP&P (365°C)	J2-354-IGT-3	3.49	751	3.36	14.8	1.8	20.6	6.9	1.91	2.0(±0.23)	7.2(±1.0, *3*)	-
	J2-354-CGT-Y	49.5	nd	6.20	1.5	0.09	nd	0.4	0.18	0.74(±0.38)	1.1(±0.1, *3*)	-
	Endmember	**0**	**766**	**3.36**	**15.9**	**2.0**	**21.9**	**7.4**	**2.05**	2.2	**7.8**	**$3.5x10^2$**
Stylo 2 (X11) (364°C)	J2-355-IGT-4	3.97	743	3.12	15.4	1.8	19.7	6.3	1.94	2.4(±0.37)	12.0(±2.4, *3*)	-
	J2-355-CGT-R	9.11	729	3.67	13.6	1.7	17.4	5.9	1.73	1.7(±0.09)	5.7(±0.5, *3*)	-
	Endmember	**0**	**763**	**3.12**	**16.5**	**2.0**	**20.9**	**7.0**	**2.10**	2.4	**10.3**	**$4.0x10^2$**
Intermediate Temperature Fluids												
Ecurie (191°C)	J2-354-IGT-4	33.8	631	5.05	4.8	0.6	11.2	2.7	0.88	2.4(±0.18)	93.3(±6.2, *4*)	-
	J2-354-IGT-8	13.2	**717**	**3.23**	**9.4**	**1.4**	**18.7**	**5.9**	**1.79**	2.4(±0.36)	**223**(±11, *3*)	**$1.3x10^6$**
Mussel Beach (180°C)	J2-355-IGT-8	7.18	**728**	**3.00**	**13.4**	**1.5**	**21.8**	**7.3**	**1.80**	1.6(±0.14)	**47.7**(±4, *3*)	**$1.5x10^6$**
Bottom Seawater		52.5	547	~8	0	0	2.2	0	0	0.1	0 (nd‡)	-
LOST CITY (750m, 30°07.4'N–42°07.2'W)												
Endmember Fluids												
Poseidon Beehive (94°C)	J2-361-CGT-B	6.50	nd §	10.2	9.1	0.21	nd	BD	0.93	3.2(±0.34)	1.6(±0.6, *3*)	-
	J2-361-CGT-W	2.30	nd §	10.5	10.1	0.47	0.19	BD	1.04	3.3(±0.17)	2.5(±1.5, *4*)	-
	J2-361-IGT-5	1.40	nd §	10.5	10.1	0.07	0.32	BD	1.06	3.3(±0.16)	1.4(±0.9, *4*)	-
	Endmember	**0**	**nd §**	**10.2**	**10.4**	**0.27**	**0.18**	BD	**1.08**	3.5	**1.9**	**nd***
Marker 6 (96°C)	J2-362-IGT-4	1.23	nd §	10.5	10.3	0.22	0.15	BD	1.10	3.4(±0.17)	1.3(±0.4, *3*)	-
	Endmember	**0**	**nd §**	**10.5**	**10.5**	**0.22**	**0.10**	BD	**1.13**	3.5	**1.4**	**nd***
Bottom Seawater		53.3	547	~8	0	0	2.2	0	0	0.1	0 (nd‡)	-
LUCKY STRIKE (1700m, 37°17.5'N–32°16.7'W)												
Endmember Fluids												
Isabel (292°C)	J2-357-IGT-5	2.75	490	3.81	0.032	3.5	106	BD	0.82	5.8(±0.31)	6.1(±1.7, *3*)	-
	Endmember	**0**	**487**	**3.81**	**0.034**	**3.7**	**112**	BD	**0.86**	6.2	**6.5**	**$1.1x10^{-2}$**
US4 (299°C)	J2-357-IGT-3	2.32	418	3.89	0.051	3.6	127	BD	0.71	8.9(±0.45)	5.3(±1.3, *4*)	-
	Endmember	**0**	**414**	**3.89**	**0.053**	**3.8**	**133**	BD	**0.74**	9.3	**5.6**	**$2.6x10^{-2}$**
Crystal (308°C)	J2-358-IGT-8	2.85	538	4.43	0.037	3.7	110	BD	0.77	16.1(±0.80)	23.0(±3.0, *3*)	-
	J2-358-CGT-R	31.2	544	4.72	0.020	2.0	48.9	BD	0.33	4.2(±0.21)	7.5(±0.9, *4*)	-
	Endmember	**0**	**538**	**4.43**	**0.041**	**4.1**	**117**	BD	**0.82**	16.0	**23.4**	**$4.3x10^{-3}$**
Medea (270°C)	J2-359-IGT-2	4.17	552	3.81	0.060	2.5	90.3	BD	0.82	6.2(±0.52)	5.4(±0.7, *3*)	-
	J2-359-CGT-Y	3.82	553	3.90	0.056	2.9	91.2	BD	0.82	5.6(±0.28)	5.6(±0.7, *3*)	-
	Endmember	**0**	**554**	**3.81**	**0.063**	**2.9**	**98.0**	BD	**0.89**	6.4	**5.9**	**$3.5x10^{-1}$**
Bottom Seawater		52.5	547	~8	0	0	2.2	0	0	0.1	0 (nd‡)	-
TAG (3600m, 26°08'N–44°49'W)												
Endmember Fluids												
Black Smoker Complex (363°C)	J2-363-IGT-5	3.93	nd §	3.28	0.095	4.7	4.94	BD	0.13	4.0(±0.65)	11.6(±2.5, *3*)	-
	J2-363-CGT-R	5.93	nd §	4.09	0.088	4.5	4.47	BD	0.13	4.4(±0.23)	10.2(±0.5, *2*)	-
	Endmember	**0**	**nd §**	**3.28**	**0.10**	**5.1**	**4.97**	BD	**0.14**	4.6	**12.0**	**$5.8x10^{-5}$**
Bottom Seawater		52.5	547	~8	0	0	2.2	0	0	0.1	0 (nd‡)	-
9°50'N EPR (2500m, 9°50.3'N–104°17.5'W)												
Endmember Fluids												
Bio9 (HOBO) (363°C)	4469-IGT-4	3.27	375	3.50	0.92	10.2	86.9	1.6	0.076	3.2(±0.16)	4.3(±0.8, *3*)	-
	4469-IGT-5	3.04	378	3.55	0.87	11.0	86.7	nd	0.075	2.3(±0.17)	3.2(±0.3, *3*)	-
	Endmember	**0**	**366**	**3.50**	**0.95**	**11.3**	**92.1**	**1.8**	**0.081**	2.9	**4.0**	**2.0**
Trick or Treat (Marker 28) (281°C)	4469-IGT-1	5.73	195	3.94	1.0	17.1	60.4	nd	0.058	1.9(±0.09)	11.1(±3, *3*)	-
	4469-IGT-3	2.45	169	3.83	1.2	18.3	66.1	1.9	0.066	2.5(±0.24)	10.0(±0.8, *3*)	-
	Endmember	**0**	**152**	**3.83**	**1.2**	**19.2**	**68.3**	**2.0**	**0.067**	2.4	**11.4**	**$4.1x10^3$**
Tica (275°C)	4464-IGT-1	4.08	335	3.83	0.37	8.2	92.5	0.81	0.091	2.1(±0.15)	3.6(±0.6, *3*)	-
	4464-IGT-6	14.4	377	4.32	0.29	6.8	72.4	0.64	0.095	2.2(±0.44)	2.9(±0.5, *3*)	-
	Endmember	**0**	**318**	**3.83**	**0.40**	**9.0**	**99.3**	**0.9**	**0.11**	2.6	**4.0**	**$1.8x10^2$**
L Vent (246°C)	4467-IGT-1	4.29	567	3.83	0.72	5.2	8.81	0.20	0.071	3.1(±0.31)	7.8(±0.4, *2*)	-
	4467-IGT-5	8.89	559	4.31	0.70	4.6	8.18	0.18	0.070	2.6(±0.24)	9.8(±0.6, *3*)	-
	Endmember	**0**	**567**	**3.83**	**0.81**	**5.6**	**9.38**	**0.22**	**0.080**	3.2	**9.9**	**$1.5x10^3$**
L Vent (Marker 8) (221°C)	4468-IGT-4	9.11	558	4.20	0.63	4.7	8.19	BD	0.066	4.0(±0.20)	7.5(±0.6, *3*)	-
	Endmember	**0**	**562**	**4.20**	**0.75**	**5.7**	**9.43**	BD	**0.080**	4.9	**9.0**	**$1.3x10^4$**

Table S1. (continued)

SITE (depth, location) Vent (Max. temp. °C)	Sample	Mg (mm)	Cl (mm)	pH (25°C)	H_2 (mM)	H_2S (mM)	ΣCO_2 (mm)	CO (µM)	CH_4 (mM)	NH_4^+ (µm (±2s))	Measured CH_3SH (nM (±2s, *n*))	Predicted CH_3SH molal
9°50'N EPR (continued)												
Intermediate Temperature & Mixed Fluids												
L Vent Fissure (78°C)	4467-IGT-6	41.1	**543**	**5.77**	**0.028**	**1.0**	**3.93**	BD	**0.037**	7.6 (±0.61)	**17.8**(±1.3, *3*)	**$7.5x10^3$**
	4467-IGT-8	49.0	nd	6.43	0.013	nd	2.96	BD	0.010	1.4 (±0.07)	6.5 (±0.3, *3*)	-
Crab Spa (23°C)	4464-IGT-4	50.3	**525**	**5.74**	**0.0032**	**0.17**	**7.26**	BD	**0.010**	8.6 (±0.72)	**6.1** (±0.3, *3*)	**$9.4x10^2$**
	4464-IGT-5	50.5	528	5.87	0.0028	0.19	7.26	BD	0.012	10.0 (±0.67)	5.7 (±0.3, *3*)	-
	4466-IGT-3	50.0	526	5.79	0.0058	0.29	7.47	BD	0.009	8.7 (±0.44)	5.9 (±0.3, *1*)	-
Bottom Seawater		53.5	538	~8	0	0	2.18	0	0	0.1	0 (nd‡)	-
GUAYMAS BASIN (2000m, 27°02'N–111°24'W)												
Endmember Fluids												
Theme Park (251°C)	4458-IGT-1	3.46	598	5.78	0.50	6.4	43.9	nd	41.5	$12.3x10^3$(±$0.62x10^3$)	$15.3x10^3$(±$0.76x10^3$, *2*)	-
	4458-IGT-8	31.9	564	5.73	0.23	2.8	21.1	nd	18.8	$5.2x10^3$ (±$0.26x10^3$)	$6.52x10^3$(±$0.80x10^3$, *3*)	-
	Endmember	**0**	**602**	**5.73**	**0.54**	**6.8**	**47.1**	nd	**44.7**	$13.1x10^3$	**$16.3x10^3$**	**nd***
Cathedral Hill (172°C)	4459-IGT-5	41.0	555	5.73	0.12	1.8	9.85	6.3	10.3	$2.8x10^3$ (±$0.14x10^3$)	$3.49x10^3$(±$0.20x10^3$, *3*)	-
	Endmember	**0**	**611**	**5.73**	**0.52**	**7.9**	**35.0**	**27**	**44.2**	$11.8x10^3$	**$14.9x10^3$**	**nd***
Sulfide Spires (218°C)	4461-IGT-5	12.9	588	5.75	0.42	5.3	31.8	76	32.8	$10.5x10^3$(±$0.53x10^3$)	$12.9x10^3$(±$1.9x10^3$, *3*)	-
	4461-IGT-8	32.3	567	4.48	0.24	2.9	21.0	26	19.3	$5.4x10^3$ (±$0.27x10^3$)	$6.14x10^3$(±$0.80x10^3$, *3*)	-
	Endmember	**0**	**605**	**4.48**	**0.56**	**7.1**	**42.9**	**92.4**	**44.4**	$13.8x10^3$	**$16.7x10^3$**	**nd***
Toadstool (288°C)	4462-IGT-5	11.3	583	6.13	2.1	6.1	41.8	nd	49.7	$12.7x10^3$(±$0.64x10^3$)	8.5(±1.0, *2*)	-
	4462-IGT-6	2.42	595	6.09	2.6	7.9	47.6	nd	61.0	$15.2x10^3$(±$0.76x10^3$)	6.1(±2.0, *2*)	-
	Endmember	**0**	**597**	**6.09**	**2.7**	**8.0**	**50.8**	nd	**63.5**	$16.0x10^3$	**8.1**	**nd***
Rebecca's Roost (299°C)	4462-IGT-1	3.12	597	6.14	3.1	7.5	45.8	nd	54.5	$14.6x10^3$(±$0.73x10^3$)	14.1(±0.7, *1*)	-
	4462-IGT-4	5.64	592	6.09	3.0	7.3	43.6	nd	53.6	$13.8x10^3$(±$0.69x10^3$)	5.1(±0.3, *1*)	-
	Endmember	**0**	**600**	**6.09**	**3.3**	**8.0**	**48.5**	nd	**58.8**	$15.5x10^3$	**11**	**nd***
Bottom Seawater		53.5	538	~8	0	0	2.18	0	0	0.1	0 (nd‡)	-
VON DAMM (2300m, 18°22.6'N–81°47.9'W)												
Endmember Fluids												
East Summit (226°C)	J2-616-IGT8	2.43	653	5.56	18.3	3.1	2.75	nd	2.71	17.1(±0.85)	21(±8.0, *2*)	-
	Endmember	**0**	**658**	**5.56**	**19.2**	**3.2**	**2.78**	nd	**2.84**	17.9	**22**	**$1.6x10^6$**
Intermediate Temperature & Mixed Fluids												
Arrow Loop #1 (134°C)	J2-616-IGT6	18.5	**615**	**5.86**	**10.8**	**1.9**	**2.27**	nd	**1.73**	14.4(±0.72)	**91.6**(±6.3, *3*)	**$1.8x10^6$**
White Castle (151°C)	J2-616-IGT1	13.5	**631**	**5.77**	**13.1**	**2.1**	**2.51**	nd	**2.08**	14.5(±0.73)	**152** (±9.2, *3*)	**$2.0x10^6$**
Ginger Castle (128°C)	J2-617-IGT4	18.0	**624**	**6.06**	**11.3**	**2.1**	**2.35**	nd	**1.91**	15.6(±0.78)	**104** (±11, *3*)	**$2.0x10^6$**
Ravelin #1 (145°C)	J2-617-IGT2	16.8	618	5.93	13.1	1.7	2.40	nd	1.98	14.2(±0.71)	57.4(±4.4, *2*)	-
	J2-617-IGT6	15.0	**625**	**5.83**	**13.4**	**2.5**	**2.52**	nd	**2.06**	14.6(±0.73)	**52.5**(±3.0, *3*)	**$2.3x10^6$**
Ravelin #2 (116°C)	J2-621-IGT2	13.4	**640**	**5.88**	**13.6**	**2.2**	**1.98**	nd	**2.14**	nd	**206** (±10, *2*)	**$1.9x10^6$**
	J2-621-IGT8	22.0	609	6.12	10.9	1.9	1.88	nd	1.73	11.2(±0.56)	154 (±11, *2*)	-
West Summit (126°C)	J2-621-IGT1	24.0	607	6.00	9.9	1.9	2.08	nd	1.64	14.1(±0.71)	142 (±7.1, *2*)	-
	J2-621-IGT4	23.2	**611**	**6.01**	**9.9**	**1.8**	**2.11**	nd	**1.67**	13.7(±0.68)	**138** (±6.9, *2*)	**$1.7x10^6$**
Bottom Seawater		52.4	545	~8	0	0	2.2	0	0	0.1	0 (nd‡)	-
PICCARD (4960m, 18°32.8'N–81°43.1'W)												
Endmember Fluids												
Beebe 3 (397°C)	J2-619-IGT4	1.26	363	3.23	20.2	11.9	25.7	nd	0.120	33.6(±2.2)	10.2(±2.3, *3*)	-
	J2-619-IGT8	1.59	363	3.17	20.1	11.4	25.0	nd	0.119	33.8(±1.7)	15.5(±8.4, *3*)	-
	Endmember	**0**	**358**	**3.17**	**20.7**	**12.0**	**26.0**	nd	**0.123**	34.7	**13.2**	**$5.3x10^2$**
Beebe Woods (354°C)	J2-618-IGT2	2.95	nd	3.24	19.6	11.6	24.5	nd	0.122	35.1(±1.8)	9.9(±0.49, *2*)	-
	J2-618-IGT8	2.97	365	3.18	19.4	11.6	24.7	nd	0.120	35.0(±1.8)	10.1(±0.81, *3*)	-
	Endmember	**0**	**354**	**3.18**	**20.7**	**12.3**	**25.9**	nd	**0.128**	37.2	**10.6**	**$1.3x10^4$**
Mixed Fluids												
Hot Chimlet #1 (149°C)	J2-619-IGT6	35.4	487	5.06	2.0	2.7	9.09	nd	0.054	14.2(±0.71)	$1.76x10^3$(±$0.11x10^3$, *3*)	-
	J2-619-IGT3	33.4	**479**	**4.97**	**2.1**	**2.3**	**10.1**	nd	**0.060**	16.9(±0.85)	**$1.76x10^3$**(±$0.21x10^3$, *3*)**$6.1x10^5$**	
Hot Chimlet #2 (95°C)	J2-620-IGT4	45.4	527	**5.67**	**0.70**	**0.98**	**4.89**	nd	**0.022**	6.2 (±0.31)	**430**(±22, *2*)	**$2.2x10^5$**
	J2-620-IGT8	47.8	**524**	5.94	0.53	0.79	4.08	nd	0.016	2.5 (±0.33)	292(±15, *2*)	-
Shrimp Gulley (45°C)	J2-618-IGT1	47.4	**530**	**5.95**	**0.12**	**0.72**	**3.39**	nd	**0.011**	2.9 (±0.58)	**50.4**(±2.5, *3*)	**$3.9x10^4$**
	J2-618-IGT3	48.9	533	5.94	0.13	1.0	3.64	nd	0.011	0.53(±0.48)	44.0(±7.1, *3*)	-
Near Shrimp Gulley (111°C)	J2-620-IGT1	42.4	**515**	**5.49**	**0.41**	**1.7**	**5.95**	nd	**0.025**	7.7 (±0.85)	**144**(±7.2, *2*)	**$1.2x10^5$**
	J2-620-IGT2	44.8	519	5.58	0.28	1.4	5.56	nd	0.021	3.4 (±0.76)	83.4(±4.2, *2*)	-
Bottom Seawater		52.4	545	~8	0	0	2.2	0	0	0.1	0 (nd‡)	-

SI Text References

1. Bischoff JL & Dickson FW (1975) Seawater-basalt interaction at 200°C and 500 bars: Implications for origin of sea-floor heavy-metal deposits and regulation of seawater chemistry. *Earth Planet. Sci. Lett.* 25:385-397.
2. Mottl MJ & Holland HD (1978) Chemical exchange during hydrothermal alteration of basalt by seawater-I. Experimental results for major and minor components of seawater. *Geochim. Cosmochim. Acta* 42(8):1103-1115.
3. Seyfried WE & Bischoff JL (1981) Experimental seawater-basalt interaction at 300°C, 500 bars, chemical exchange, secondary mineral formation and implications for the transport of heavy metals. *Geochim. Cosmochim. Acta* 45(2):135-147.
4. Von Damm KL, Edmond JM, Grant B, & Measures CI (1985) Chemistry of submarine hydrothermal solutions at 21°N, East Pacific Rise. *Geochim. Cosmochim. Acta* 49(11):2197-2220.
5. Reeves EP*, et al.* (2011) Geochemistry of hydrothermal fluids from the PACMANUS, Northeast Pual and Vienna Woods hydrothermal fields, Manus Basin, Papua New Guinea. *Geochim. Cosmochim. Acta* 75:1088–1123.
6. Shock EL & Helgeson HC (1990) Calculation of the thermodynamic and transport properties of aqueous species at high pressures and temperatures: Standard partial molal properties of organic species. *Geochim. Cosmochim. Acta* 54(4):915-945.
7. Seewald JS (2001) Aqueous geochemistry of low molecular weight hydrocarbons at elevated temperatures and pressures: Constraints from mineral buffered laboratory experiments. *Geochim. Cosmochim. Acta* 65(10):1641-1664.
8. Seewald JS, Zolotov MY, & McCollom T (2006) Experimental investigation of single carbon compounds under hydrothermal conditions. *Geochim. Cosmochim. Acta* 70(2):446-460.
9. Amend JP, McCollom TM, Hentscher M, & Bach W (2011) Catabolic and anabolic energy for chemolithoautotrophs in deep-sea hydrothermal systems hosted in different rock types. *Geochim. Cosmochim. Acta* 75(19):5736-5748.
10. Schulte MD & Rogers KL (2004) Thiols in hydrothermal solution: standard partial molal properties and their role in the organic geochemistry of hydrothermal environments. *Geochim. Cosmochim. Acta* 68(5):1087-1097.
11. Proskurowski G*, et al.* (2008) Abiogenic hydrocarbon production at Lost City hydrothermal field. *Science* 319(5863):604-607.

12. Anderson G (2005) *Thermodynamics of Natural Systems* (Cambridge Univ. Press) 2 Ed.
13. Proskurowski G, Lilley MD, & Olson EJ (2008) Stable isotopic evidence in support of active microbial methane cycling in low-temperature diffuse flow vents at 9°50'N East Pacific Rise. *Geochim. Cosmochim. Acta* 72(8):2005-2023.
14. Seyfried WE, Pester NJ, Ding K, & Rough M (2011) Vent fluid chemistry of the Rainbow hydrothermal system (36°N, MAR): Phase equilibria and in situ pH controls on subseafloor alteration processes. *Geochim. Cosmochim. Acta* 75(6):1574-1593.
15. Pester NJ*, et al.* (2012) Subseafloor phase equilibria in high-temperature hydrothermal fluids of the Lucky Strike Seamount (Mid-Atlantic Ridge, 37°17'N). *Geochim. Cosmochim. Acta* 90:303-322.
16. Lam P, Cowen JP, & Jones RD (2004) Autotrophic ammonia oxidation in a deep-sea hydrothermal plume. *FEMS Microbiol. Ecol.* 47(2):191-206.
17. Foustoukos DI & Seyfried WE (2005) Redox and pH constraints in the subseafloor root zone of the TAG hydrothermal system, 26° N Mid-Atlantic Ridge. *Earth Planet. Sci. Lett.* 235(3-4):497-510.

Table S1. Measured and calculated endmember concentrations of dissolved species

SITE (depth, location) Vent (Max. temp. °C)	Sample	Mg (mm)	Cl (mm)	pH (25°C)	H_2 (mM)	H_2S (mM)	ΣCO_2 (mm)	CO (µM)	CH_4 (mM)	NH_4^+ (µm (±2s))	Measured CH_3SH (nM (±2s, *n*))	Predicted CH_3SH nmolal
RAINBOW (2300m, 36°13.80'N–33°54.15'W)												
Endmember Fluids												
PP27/Exo2/Padraig/Termitiere (350°C)	J2-353-IGT-3	6.90	732	3.35	10.7	2.7	19.6	4.5	1.73	1.8(±0.28)	6.7(±0.3, *1*)	-
	J2-353-CGT-R	7.05	728	3.59	10.6	3.0	17.8	4.4	1.76	2.9(±0.15)	6.5(±0.3, *1*)	-
	Endmember	**0**	**758**	**3.35**	**12.3**	**3.3**	**21.3**	**5.1**	**2.01**	2.7	**7.7**	**$8.0x10^2$**
Stylo 1 (367°C)	J2-354-IGT-5	4.17	746	3.31	15.0	1.9	23.4	6.6	1.95	1.9(±0.21)	7.6(±0.8, *4*)	-
	J2-354-CGT-B	3.92	750	3.39	14.8	2.3	22.3	6.8	1.93	2.3(±0.23)	6.1(±0.9, *3*)	-
	Endmember	**0**	**765**	**3.31**	**16.1**	**2.3**	**24.6**	**7.2**	**2.10**	2.3	**7.4**	**$4.0x10^2$**
CMSP&P (365°C)	J2-354-IGT-3	3.49	751	3.36	14.8	1.8	20.6	6.9	1.91	2.0(±0.23)	7.2(±1.0, *3*)	-
	J2-354-CGT-Y	49.5	nd	6.20	1.5	0.09	nd	0.4	0.18	0.74(±0.38)	1.1(±0.1, *3*)	-
	Endmember	**0**	**766**	**3.36**	**15.9**	**2.0**	**21.9**	**7.4**	**2.05**	2.2	**7.8**	**$3.5x10^2$**
Stylo 2 (X11) (364°C)	J2-355-IGT-4	3.97	743	3.12	15.4	1.8	19.7	6.3	1.94	2.4(±0.37)	12.0(±2.4, *3*)	-
	J2-355-CGT-R	9.11	729	3.67	13.6	1.7	17.4	5.9	1.73	1.7(±0.09)	5.7(±0.5, *3*)	-
	Endmember	**0**	**763**	**3.12**	**16.5**	**2.0**	**20.9**	**7.0**	**2.10**	2.4	**10.3**	**$4.0x10^2$**
Intermediate Temperature Fluids												
Ecurie (191°C)	J2-354-IGT-4	33.8	631	5.05	4.8	0.6	11.2	2.7	0.88	2.4(±0.18)	93.3(±6.2, *4*)	-
	J2-354-IGT-8	13.2	**717**	**3.23**	**9.4**	**1.4**	**18.7**	**5.9**	**1.79**	2.4(±0.36)	**223**(±11, *3*)	**$1.3x10^6$**
Mussel Beach (180°C)	J2-355-IGT-8	7.18	**728**	**3.00**	**13.4**	**1.5**	**21.8**	**7.3**	**1.80**	1.6(±0.14)	**47.7**(±4, *3*)	**$1.5x10^6$**
Bottom Seawater		52.5	547	~8	0	0	2.2	0	0	0.1	0 (nd‡)	-
LOST CITY (750m, 30°07.4'N–42°07.2'W)												
Endmember Fluids												
Poseidon Beehive (94°C)	J2-361-CGT-B	6.50	nd §	10.2	9.1	0.21	nd	BD	0.93	3.2(±0.34)	1.6(±0.6, *3*)	-
	J2-361-CGT-W	2.30	nd §	10.5	10.1	0.47	0.19	BD	1.04	3.3(±0.17)	2.5(±1.5, *4*)	-
	J2-361-IGT-5	1.40	nd §	10.5	10.1	0.07	0.32	BD	1.06	3.3(±0.16)	1.4(±0.9, *4*)	-
	Endmember	**0**	**nd §**	**10.2**	**10.4**	**0.27**	**0.18**	BD	**1.08**	3.5	**1.9**	**nd***
Marker 6 (96°C)	J2-362-IGT-4	1.23	nd §	10.5	10.3	0.22	0.15	BD	1.10	3.4(±0.17)	1.3(±0.4, *3*)	-
	Endmember	**0**	**nd §**	**10.5**	**10.5**	**0.22**	**0.10**	BD	**1.13**	3.5	**1.4**	**nd***
Bottom Seawater		53.3	547	~8	0	0	2.2	0	0	0.1	0 (nd‡)	-
LUCKY STRIKE (1700m, 37°17.5'N–32°16.7'W)												
Endmember Fluids												
Isabel (292°C)	J2-357-IGT-5	2.75	490	3.81	0.032	3.5	106	BD	0.82	5.8(±0.31)	6.1(±1.7, *3*)	-
	Endmember	**0**	**487**	**3.81**	**0.034**	**3.7**	**112**	BD	**0.86**	6.2	**6.5**	**$1.1x10^{-2}$**
US4 (299°C)	J2-357-IGT-3	2.32	418	3.89	0.051	3.6	127	BD	0.71	8.9(±0.45)	5.3(±1.3, *4*)	-
	Endmember	**0**	**414**	**3.89**	**0.053**	**3.8**	**133**	BD	**0.74**	9.3	**5.6**	**$2.6x10^{-2}$**
Crystal (308°C)	J2-358-IGT-8	2.85	538	4.43	0.037	3.7	110	BD	0.77	16.1(±0.80)	23.0(±3.0, *3*)	-
	J2-358-CGT-R	31.2	544	4.72	0.020	2.0	48.9	BD	0.33	4.2(±0.21)	7.5(±0.9, *4*)	-
	Endmember	**0**	**538**	**4.43**	**0.041**	**4.1**	**117**	BD	**0.82**	16.0	**23.4**	**$4.3x10^{-3}$**
Medea (270°C)	J2-359-IGT-2	4.17	552	3.81	0.060	2.5	90.3	BD	0.82	6.2(±0.52)	5.4(±0.7, *3*)	-
	J2-359-CGT-Y	3.82	553	3.90	0.056	2.9	91.2	BD	0.82	5.6(±0.28)	5.6(±0.7, *3*)	-
	Endmember	**0**	**554**	**3.81**	**0.063**	**2.9**	**98.0**	BD	**0.89**	6.4	**5.9**	**$3.5x10^{-1}$**
Bottom Seawater		52.5	547	~8	0	0	2.2	0	0	0.1	0 (nd‡)	-
TAG (3600m, 26°08'N–44°49'W)												
Endmember Fluids												
Black Smoker Complex (363°C)	J2-363-IGT-5	3.93	nd §	3.28	0.095	4.7	4.94	BD	0.13	4.0(±0.65)	11.6(±2.5, *3*)	-
	J2-363-CGT-R	5.93	nd §	4.09	0.088	4.5	4.47	BD	0.13	4.4(±0.23)	10.2(±0.5, *2*)	-
	Endmember	**0**	**nd §**	**3.28**	**0.10**	**5.1**	**4.97**	BD	**0.14**	4.6	**12.0**	**$5.8x10^{-5}$**
Bottom Seawater		52.5	547	~8	0	0	2.2	0	0	0.1	0 (nd‡)	-
9°50'N EPR (2500m, 9°50.3'N–104°17.5'W)												
Endmember Fluids												
Bio9 (HOBO) (363°C)	4469-IGT-4	3.27	375	3.50	0.92	10.2	86.9	1.6	0.076	3.2(±0.16)	4.3(±0.8, *3*)	-
	4469-IGT-5	3.04	378	3.55	0.87	11.0	86.7	nd	0.075	2.3(±0.17)	3.2(±0.3, *3*)	-
	Endmember	**0**	**366**	**3.50**	**0.95**	**11.3**	**92.1**	**1.8**	**0.081**	2.9	**4.0**	**2.0**
Trick or Treat (Marker 28) (281°C)	4469-IGT-1	5.73	195	3.94	1.0	17.1	60.4	nd	0.058	1.9(±0.09)	11.1(±3, *3*)	-
	4469-IGT-3	2.45	169	3.83	1.2	18.3	66.1	1.9	0.066	2.5(±0.24)	10.0(±0.8, *3*)	-
	Endmember	**0**	**152**	**3.83**	**1.2**	**19.2**	**68.3**	**2.0**	**0.067**	2.4	**11.4**	**$4.1x10^3$**
Tica (275°C)	4464-IGT-1	4.08	335	3.83	0.37	8.2	92.5	0.81	0.091	2.1(±0.15)	3.6(±0.6, *3*)	-
	4464-IGT-6	14.4	377	4.32	0.29	6.8	72.4	0.64	0.095	2.2(±0.44)	2.9(±0.5, *3*)	-
	Endmember	**0**	**318**	**3.83**	**0.40**	**9.0**	**99.3**	**0.9**	**0.11**	2.6	**4.0**	**$1.8x10^2$**
L Vent (246°C)	4467-IGT-1	4.29	567	3.83	0.72	5.2	8.81	0.20	0.071	3.1(±0.31)	7.8(±0.4, *2*)	-
	4467-IGT-5	8.89	559	4.31	0.70	4.6	8.18	0.18	0.070	2.6(±0.24)	9.8(±0.6, *3*)	-
	Endmember	**0**	**567**	**3.83**	**0.81**	**5.6**	**9.38**	**0.22**	**0.080**	3.2	**9.9**	**$1.5x10^3$**
L Vent (Marker 8) (221°C)	4468-IGT-4	9.11	558	4.20	0.63	4.7	8.19	BD	0.066	4.0(±0.20)	7.5(±0.6, *3*)	-
	Endmember	**0**	**562**	**4.20**	**0.75**	**5.7**	**9.43**	BD	**0.080**	4.9	**9.0**	**$1.3x10^4$**

Table S1. (continued)

SITE (depth, location) Vent (Max. temp. °C)	Sample	Mg (mm)	Cl (mm)	pH (25°C)	H_2 (mM)	H_2S (mM)	ΣCO_2 (mm)	CO (µM)	CH_4 (mM)	NH_4^+ (µm (±2s))	Measured CH_3SH (nM (±2s, *n*))	Predicted CH_3SH molal
9°50'N EPR (continued)												
Intermediate Temperature & Mixed Fluids												
L Vent Fissure (78°C)	4467-IGT-6	41.1	**543**	**5.77**	**0.028**	**1.0**	**3.93**	BD	**0.037**	7.6 (±0.61)	**17.8**(±1.3, *3*)	**$7.5x10^3$**
	4467-IGT-8	49.0	nd	6.43	0.013	nd	2.96	BD	0.010	1.4 (±0.07)	6.5 (±0.3, *3*)	-
Crab Spa (23°C)	4464-IGT-4	50.3	**525**	**5.74**	**0.0032**	**0.17**	**7.26**	BD	**0.010**	8.6 (±0.72)	**6.1** (±0.3, *3*)	**$9.4x10^2$**
	4464-IGT-5	50.5	528	5.87	0.0028	0.19	7.26	BD	0.012	10.0 (±0.67)	5.7 (±0.3, *3*)	-
	4466-IGT-3	50.0	526	5.79	0.0058	0.29	7.47	BD	0.009	8.7 (±0.44)	5.9 (±0.3, *1*)	-
Bottom Seawater		53.5	538	~8	0	0	2.18	0	0	0.1	0 (nd‡)	-
GUAYMAS BASIN (2000m, 27°02'N–111°24'W)												
Endmember Fluids												
Theme Park (251°C)	4458-IGT-1	3.46	598	5.78	0.50	6.4	43.9	nd	41.5	$12.3x10^3$(±$0.62x10^3$)	$15.3x10^3$(±$0.76x10^3$, *2*)	-
	4458-IGT-8	31.9	564	5.73	0.23	2.8	21.1	nd	18.8	$5.2x10^3$ (±$0.26x10^3$)	$6.52x10^3$(±$0.80x10^3$, *3*)	-
	Endmember	**0**	**602**	**5.73**	**0.54**	**6.8**	**47.1**	nd	**44.7**	$13.1x10^3$	**$16.3x10^3$**	**nd***
Cathedral Hill (172°C)	4459-IGT-5	41.0	555	5.73	0.12	1.8	9.85	6.3	10.3	$2.8x10^3$ (±$0.14x10^3$)	$3.49x10^3$(±$0.20x10^3$, *3*)	-
	Endmember	**0**	**611**	**5.73**	**0.52**	**7.9**	**35.0**	**27**	**44.2**	$11.8x10^3$	**$14.9x10^3$**	**nd***
Sulfide Spires (218°C)	4461-IGT-5	12.9	588	5.75	0.42	5.3	31.8	76	32.8	$10.5x10^3$(±$0.53x10^3$)	$12.9x10^3$(±$1.9x10^3$, *3*)	-
	4461-IGT-8	32.3	567	4.48	0.24	2.9	21.0	26	19.3	$5.4x10^3$ (±$0.27x10^3$)	$6.14x10^3$(±$0.80x10^3$, *3*)	-
	Endmember	**0**	**605**	**4.48**	**0.56**	**7.1**	**42.9**	**92.4**	**44.4**	$13.8x10^3$	**$16.7x10^3$**	**nd***
Toadstool (288°C)	4462-IGT-5	11.3	583	6.13	2.1	6.1	41.8	nd	49.7	$12.7x10^3$(±$0.64x10^3$)	8.5(±1.0, *2*)	-
	4462-IGT-6	2.42	595	6.09	2.6	7.9	47.6	nd	61.0	$15.2x10^3$(±$0.76x10^3$)	6.1(±2.0, *2*)	-
	Endmember	**0**	**597**	**6.09**	**2.7**	**8.0**	**50.8**	nd	**63.5**	$16.0x10^3$	**8.1**	**nd***
Rebecca's Roost (299°C)	4462-IGT-1	3.12	597	6.14	3.1	7.5	45.8	nd	54.5	$14.6x10^3$(±$0.73x10^3$)	14.1(±0.7, *1*)	-
	4462-IGT-4	5.64	592	6.09	3.0	7.3	43.6	nd	53.6	$13.8x10^3$(±$0.69x10^3$)	5.1(±0.3, *1*)	-
	Endmember	**0**	**600**	**6.09**	**3.3**	**8.0**	**48.5**	nd	**58.8**	$15.5x10^3$	**11**	**nd***
Bottom Seawater		53.5	538	~8	0	0	2.18	0	0	0.1	0 (nd‡)	-
VON DAMM (2300m, 18°22.6'N–81°47.9'W)												
Endmember Fluids												
East Summit (226°C)	J2-616-IGT8	2.43	653	5.56	18.3	3.1	2.75	nd	2.71	17.1(±0.85)	21(±8.0, *2*)	-
	Endmember	**0**	**658**	**5.56**	**19.2**	**3.2**	**2.78**	nd	**2.84**	17.9	**22**	**$1.6x10^6$**
Intermediate Temperature & Mixed Fluids												
Arrow Loop #1 (134°C)	J2-616-IGT6	18.5	**615**	**5.86**	**10.8**	**1.9**	**2.27**	nd	**1.73**	14.4(±0.72)	**91.6**(±6.3, *3*)	**$1.8x10^6$**
White Castle (151°C)	J2-616-IGT1	13.5	**631**	**5.77**	**13.1**	**2.1**	**2.51**	nd	**2.08**	14.5(±0.73)	**152** (±9.2, *3*)	**$2.0x10^6$**
Ginger Castle (128°C)	J2-617-IGT4	18.0	**624**	**6.06**	**11.3**	**2.1**	**2.35**	nd	**1.91**	15.6(±0.78)	**104** (±11, *3*)	**$2.0x10^6$**
Ravelin #1 (145°C)	J2-617-IGT2	16.8	618	5.93	13.1	1.7	2.40	nd	1.98	14.2(±0.71)	57.4(±4.4, *2*)	-
	J2-617-IGT6	15.0	**625**	**5.83**	**13.4**	**2.5**	**2.52**	nd	**2.06**	14.6(±0.73)	**52.5**(±3.0, *3*)	**$2.3x10^6$**
Ravelin #2 (116°C)	J2-621-IGT2	13.4	**640**	**5.88**	**13.6**	**2.2**	**1.98**	nd	**2.14**	nd	**206** (±10, *2*)	**$1.9x10^6$**
	J2-621-IGT8	22.0	609	6.12	10.9	1.9	1.88	nd	1.73	11.2(±0.56)	154 (±11, *2*)	-
West Summit (126°C)	J2-621-IGT1	24.0	607	6.00	9.9	1.9	2.08	nd	1.64	14.1(±0.71)	142 (±7.1, *2*)	-
	J2-621-IGT4	23.2	**611**	**6.01**	**9.9**	**1.8**	**2.11**	nd	**1.67**	13.7(±0.68)	**138** (±6.9, *2*)	**$1.7x10^6$**
Bottom Seawater		52.4	545	~8	0	0	2.2	0	0	0.1	0 (nd‡)	-
PICCARD (4960m, 18°32.8'N–81°43.1'W)												
Endmember Fluids												
Beebe 3 (397°C)	J2-619-IGT4	1.26	363	3.23	20.2	11.9	25.7	nd	0.120	33.6(±2.2)	10.2(±2.3, *3*)	-
	J2-619-IGT8	1.59	363	3.17	20.1	11.4	25.0	nd	0.119	33.8(±1.7)	15.5(±8.4, *3*)	-
	Endmember	**0**	**358**	**3.17**	**20.7**	**12.0**	**26.0**	nd	**0.123**	34.7	**13.2**	**$5.3x10^2$**
Beebe Woods (354°C)	J2-618-IGT2	2.95	nd	3.24	19.6	11.6	24.5	nd	0.122	35.1(±1.8)	9.9(±0.49, *2*)	-
	J2-618-IGT8	2.97	365	3.18	19.4	11.6	24.7	nd	0.120	35.0(±1.8)	10.1(±0.81, *3*)	-
	Endmember	**0**	**354**	**3.18**	**20.7**	**12.3**	**25.9**	nd	**0.128**	37.2	**10.6**	**$1.3x10^4$**
Mixed Fluids												
Hot Chimlet #1 (149°C)	J2-619-IGT6	35.4	487	5.06	2.0	2.7	9.09	nd	0.054	14.2(±0.71)	$1.76x10^3$(±$0.11x10^3$, *3*)	-
	J2-619-IGT3	33.4	**479**	**4.97**	**2.1**	**2.3**	**10.1**	nd	**0.060**	16.9(±0.85)	**$1.76x10^3$**(±$0.21x10^3$, *3*)**$6.1x10^5$**	
Hot Chimlet #2 (95°C)	J2-620-IGT4	45.4	527	**5.67**	**0.70**	**0.98**	**4.89**	nd	**0.022**	6.2 (±0.31)	**430**(±22, *2*)	**$2.2x10^5$**
	J2-620-IGT8	47.8	**524**	5.94	0.53	0.79	4.08	nd	0.016	2.5 (±0.33)	292(±15, *2*)	-
Shrimp Gulley (45°C)	J2-618-IGT1	47.4	**530**	**5.95**	**0.12**	**0.72**	**3.39**	nd	**0.011**	2.9 (±0.58)	**50.4**(±2.5, *3*)	**$3.9x10^4$**
	J2-618-IGT3	48.9	533	5.94	0.13	1.0	3.64	nd	0.011	0.53(±0.48)	44.0(±7.1, *3*)	-
Near Shrimp Gulley (111°C)	J2-620-IGT1	42.4	**515**	**5.49**	**0.41**	**1.7**	**5.95**	nd	**0.025**	7.7 (±0.85)	**144**(±7.2, *2*)	**$1.2x10^5$**
	J2-620-IGT2	44.8	519	5.58	0.28	1.4	5.56	nd	0.021	3.4 (±0.76)	83.4(±4.2, *2*)	-
Bottom Seawater		52.4	545	~8	0	0	2.2	0	0	0.1	0 (nd‡)	-